ENVIRONMENTAL RESEARCH
CLIMATE

PURPOSE-LED PUBLISHING™

Part of the ENVIRONMENTAL RESEARCH SERIES

PAPER • **OPEN ACCESS**

South Asian monsoon response to regional aerosol emission reductions: insights from RAMIP

To cite this article: Ankit Bhandekar *et al* 2026 *Environ. Res.: Climate* **5** 035036

View the article online for updates and enhancements.

ENVIRONMENTAL RESEARCH
CLIMATE

Check for updates

OPEN ACCESS

RECEIVED
18 December 2025

REVISED
31 May 2026

ACCEPTED FOR PUBLICATION
19 June 2026

PUBLISHED
9 July 2026

PAPER

South Asian monsoon response to regional aerosol emission reductions: insights from RAMIP

Ankit Bhandekar[1,*], Laura J Wilcox[2], Bryan N Lawrence[2], Nathan Luke Abraham[3,4], Fiona M O'Connor[5,6], Bjørn H Samset[7], Robert J Allen[8], Sharar Ahmadi[2], Annica M L Ekman[9], Maxwell T Elling[10,11], Luke Fraser-Leach[12], Paul Griffiths[13], James Keeble[14], Tsuyoshi Koshiro[15], Paul Kushner[12], Anna Lewinschal[9], Molly MacRae[1,16], Risto Makkonen[17], Joonas Merikanto[17], Pierre Nabat[18], Larissa Nazarenko[19,20], Declan O'Donnell[17], Naga Oshima[15], Geeta Persad[21], Steven T Rumbold[2], Neil Swart[23], Toshihiko Takemura[22], Kostas Tsigaridis[19,20] and Daniel M Westervelt[24]

1 University of Reading Reading, United Kingdom
2 National Centre for Atmospheric Science, University of Reading, Reading, United Kingdom
3 Yusuf Hamied Department of Chemistry, University of Cambridge, Cambridge, United Kingdom
4 National Centre for Atmospheric Science,University of Cambridge, Cambridge, United Kingdom
5 Met Office Hadley Centre, Exeter, United Kingdom
6 Department of Mathematics & Statistics, Global Systems Institute, University of Exeter, Exeter, United Kingdom
7 CICERO Center for International Climate Research, Oslo, Norway
8 Department of Earth and Planetary Sciences, University of California Riverside Riverside, CA, United States of America
9 Department of Meteorology, Stockholm University, Bolin Centre for Climate Research, Stockholm, Sweden
10 Department of Atmospheric and Oceanic Sciences, University of Colorado Boulder, Boulder, CO, United States of America
11 Cooperative Institute for Research in Environmental Sciences, University of Colorado Boulder, Boulder, CO, United States of America
12 Department of Physics, University of Toronto, Toronto, Canada
13 School of Chemistry, University of Bristol Bristol, United Kingdom
14 Lancaster Environment Centre, Lancaster University Lancaster, United Kingdom
15 Meteorological Research Institute, Japan Meteorological Agency Ibaraki, Japan
16 Centre for Environmental Data Analysis, Harwell Campus, Didcot, United Kingdom
17 Finnish Meteorological Institute, Helsinki, Finland
18 Centre National de Recherches Météorologiques Toulouse, France
19 Center for Climate Systems Research, Columbia University, Palisades, NY, United States of America
20 NASA Goddard Institute of Space Studies, New York, NY, United States of America
21 Department of Geological Sciences, The University of Texas at Austin Austin, TX, United States of America
22 Research Institute for Applied Mechanics, Kyushu University Fukuoka, Japan
23 Canadian Centre for Climate Modelling and Analysis, Environment and Climate Change Canada, Victoria, BC, Canada
24 Lamont-Doherty Earth Observatory, Columbia Climate School, New York, NY, United States of America
* Author to whom any correspondence should be addressed.

E-mail: **ankit.r.bhandekar@pgr.reading.ac.uk**

Keywords: aerosols, monsoon, regional climate, India, climate change, air quality, cmip6

Supplementary material for this article is available online

Abstract

Anthropogenic aerosol and associated precursor gas emissions are already declining in many regions and are likely to decline significantly by 2050, with major implications for regional climate. Unlike greenhouse gases, aerosol impacts are spatially heterogeneous and can influence climate both near emission sources and through remote teleconnections. This is particularly important for the South Asian monsoon system, where both local and remote aerosol changes can significantly affect precipitation patterns. Using simulations from the Regional Aerosol Model Intercomparison Project, we examine how local and remote aerosol emission reductions influence South Asian climate across both pre-monsoon and monsoon seasons, including weakening of the elevated heat pump (EHP) mechanism during pre-monsoon months. Our analysis employs 10-member ensembles from 10 CMIP6-era models to compare three experiments with global, South Asian, and East Asian aerosol reductions relative to a high-emission baseline (SSP3-7.0). This experimental design allows us to isolate and quantify the distinct impacts of regional emission changes. Results reveal that global aerosol reductions produce a larger all-India precipitation increase (+0.28 mm day^{-1})

than South Asian reductions alone (+0.19 mm day^{-1}), with the strongest regional responses over the northern Bay of Bengal, the Western Ghats and Indo-Gangetic Plains. East Asian reductions show uncertain but modest precipitation reductions of 0.2–0.6 mm day^{-1} over parts of west-central and eastern Indian regions. Pre-monsoon carbonaceous aerosol reductions systematically weaken the EHP, cooling the mid-troposphere over the Himalayan foothills by up to 0.4 K and producing localised anomalous descent that opposes the climatological pre-monsoon ascent. Substantial inter-model diversity exists in the spatial patterns and magnitudes of these responses, highlighting key uncertainties in aerosol–monsoon interactions. The South Asian precipitation response is driven by enhanced land–sea thermal contrast, while the pre-monsoon EHP weakening is attributable exclusively to local South Asian carbonaceous aerosol forcing rather than remote teleconnections. These findings have direct implications for air quality and climate adaptation planning across South Asia as regional aerosol emissions diverge under different development pathways.

1. Introduction

The South Asian Summer Monsoon (SASM), which provides water resources for over a billion people, shows high sensitivity to aerosol forcing through complex radiative, microphysical, and dynamical mechanisms that vary dramatically by season, emission location, and aerosol type (Chung *et al* 2002, Ramanathan *et al* 2005, Li *et al* 2016, Liu *et al* 2024, Stier *et al* 2024). These mechanisms combine to produce a net weakening of the SASM over the historical period, contributing to observed declining precipitation trends across the Indian subcontinent (Bollasina *et al* 2011, Krishnan *et al* 2016). For example, aerosol-induced surface cooling weakens the land-sea temperature gradient that drives monsoon circulation, while Northern Hemisphere cooling from aerosols can shift the Intertropical Convergence Zone southward, reducing South Asian rainfall. However, the relative importance of these mechanisms and their interactions remain subjects of active research, particularly as they manifest differently across various temporal and spatial scales.

The seasonal evolution of aerosol-monsoon interactions reveals fundamentally different mechanisms operating during pre-monsoon versus established monsoon periods. During the pre-monsoon season (March–May), the elevated heat pump (EHP; Lau and Kim 2006) mechanism dominates aerosol effects. D'Errico *et al* (2015) demonstrate through coupled aerosol-climate modelling that enhanced pre-monsoon rainfall in April-May results from black carbon and dust accumulation over the Himalayas and Tibetan Plateau, creating upper-tropospheric warming that strengthens the meridional temperature gradient, enhancing moisture transport. This early intensification, however, triggers subsequent cooling effects that reduce July-August precipitation, illustrating complex time-lagged responses.

The transition from pre-monsoon enhancement to peak monsoon suppression reflects changing dominant physical mechanisms. Barman and Gokhale (2023) show that aerosols transported from the Indo-Gangetic Plain (IGP) to northeast India contribute 65%–80% of aerosol radiative forcing during pre-monsoon, with westerlies providing efficient transport during March–May. As the monsoon establishes, microphysical effects become increasingly important as deeper convection transports more cloud water to mixed-phase and ice levels where aerosol impacts on ice nucleation, riming, and latent heat release significantly affect cloud properties and precipitation (Fan *et al* 2016). Sarangi *et al* (2016) document that pre-monsoon atmospheric heating rates from elevated aerosol layers are 2–3 times higher than during peak monsoon, when aerosol washout reduces elevated heating and cloud-aerosol interactions dominate precipitation responses. Different aerosol types produce distinct effects: absorbing aerosols (e.g. black carbon) enhance atmospheric heating, potentially strengthening early monsoon circulation through the EHP mechanism, while scattering aerosols (e.g. sulfate) primarily cool the surface and reduce precipitation. Dave *et al* (2017) demonstrate through observational analysis that aerosols cause repeated short-term rainfall suppression during 2000–2009, acting through atmospheric stabilisation and increased moisture divergence. These effects manifest as higher frequency of prolonged rainfall breaks exceeding 7 days in high aerosol regions.

Critically, the geographic location of aerosol emissions determines both the magnitude and spatial pattern of monsoon responses through distinct atmospheric pathways (Persad 2023). The shared socioeconomic pathways (SSPs; Riahi *et al* 2017), developed to explore future climate under different societal development trajectories, project divergent aerosol emission scenarios across Asia, with substantial regional variations in both the magnitude and timing of emission changes (Lund *et al* 2019). Wilcox *et al* (2020) demonstrate that rapid aerosol reductions under SSP1-2.6 lead to accelerated monsoon precipitation increases, while continued emission growth under SSP3-7.0 significantly suppresses rainfall, particularly over South Asia. Jin *et al* (2014) demonstrate that Middle East dust aerosols enhance Indian summer monsoon rainfall on weekly timescales, with dust contributing 53% of total aerosol optical depth (AOD) over the Arabian Sea and Iranian Plateau during monsoon season. The enhancement mechanism operates through dust-induced atmospheric heating over the Iranian Plateau, which strengthens south-westerly monsoon flow. Jin *et al* (2016) quantify this sensitivity, showing dust-induced rainfall changes ranging from −9% to +23% of climatology depending on dust absorption properties.

East Asian aerosols also generally suppress South Asian monsoon precipitation, but do so through teleconnections. East Asian aerosols demonstrate the strongest remote effects per unit emission on South Asian precipitation compared to other midlatitude regions such as North America and Europe, primarily through large-scale circulation changes and inter-hemispheric temperature gradient modifications (Shawki *et al* 2018). Guo *et al* (2016) find that effects of remote East Asian emissions can rival local South Asian emissions in their impact on monsoon rainfall, with the regional response showing strong sensitivity to the geographic distribution of emission changes. Asutosh *et al* (2022) reveal that effects of remote aerosols often exceed local emission impacts, with Asian emissions showing weaker and opposing changes in global monsoon precipitation compared to other regions. Local South Asian aerosols present mixed impacts depending on composition and altitude. Herbert *et al* (2021), using idealised perturbation experiments, demonstrated strong non-linear interactions between the climate response to South and East Asian aerosol forcing, though the large magnitude and equilibrium nature of their perturbations requires careful interpretation when applying to real-world transient emission changes. Local dust aerosols generate regional precipitation declines exceeding 1 $mm\,d^{-1}$ over the central Indian region and IGP (Asutosh and Vinoj 2024). Sulfate aerosols show the strongest suppression effects, with chemistry-climate model simulations indicating that a 48% enhancement in South Asian SO_2 emissions reduces the SASM by up to 43.3% during La Niña years and 27.5% during normal years (Fadnavis *et al* 2024).

Wang *et al* (2023) reveal that under carbon neutrality scenarios, aerosol reductions will overtake greenhouse gases in driving regional climate change (particularly in Asia and regions with large historical aerosol loadings) by 2050, with frequency and intensity of extreme weather events increasing significantly. Westervelt *et al* (2020) show that aerosols are larger drivers of historical South Asian monsoon precipitation changes than greenhouse gases, highlighting the importance of understanding aerosol impacts on this critical climate system. This aerosol unmasking effect fundamentally alters traditional greenhouse gas-focused climate projections through the regionally heterogeneous nature of the forcing (Quaas *et al* 2022). The contrasting trajectories of East and South Asian emissions create a dipole pattern with profound implications for regional precipitation (Samset *et al* 2019, Xiang *et al* 2023). While East Asia experiences emission reductions enhancing northern hemisphere warming, South Asia faces continued aerosol increases resulting in weakening of the SASM. Recent observational and modeling studies suggest continued uncertainties regarding the strength and even sign of non-linear interactions between the climate responses to different aerosol types and source regions, as demonstrated by Herbert *et al* (2021), meaning that coordinated regional approaches are essential for managing these interconnected systems (Samset *et al* 2019).

Previous idealised aerosol perturbation studies, while valuable for understanding mechanisms, suffer from several key limitations that constrain their applicability to real-world emission scenarios. Experiments such as (Precipitation Driver Response Model Intercomparison Project; Liu *et al* 2018) employed artificially large perturbations in equilibrium simulations, making connections to realistic transient evolution challenging. Large emission perturbations provide clear signals of forced responses and are useful for understanding mechanisms, but cannot be linearly scaled to real-world changes because of non-linear processes such as buffering of aerosol-cloud interactions at high aerosol concentrations. Additionally, equilibrium perturbations are difficult to interpret for real-world changes because actual responses typically have not reached equilibrium, which can cause differences not only in magnitude but also in the pattern or even sign of the response if real-world changes are dominated by fast rather than slow responses. For instance, Voigt *et al* (2017) showed that fast and slow ITCZ responses to aerosols are of opposite sign, with the slow southward ITCZ shift dominating over the small fast northward ITCZ shift. Liu *et al* (2024) demonstrate that aerosol impacts are strongly modulated by model precipitation biases, with models exhibiting dry biases over India showing opposite responses compared to those with wet biases, so consideration of multiple models is preferable for identifying forced precipitation changes and their driving mechanisms. The Regional Aerosol Model Intercomparison Project (RAMIP; Wilcox *et al* 2023) builds on previous idealised perturbation studies by focusing on realistic, transient, regional aerosol emission changes for near-term projections. RAMIP employs plausible future emission trajectories from the SSPs, focusing on four key regions with the largest emission uncertainties: East Asia, South Asia, Africa/Middle East, and North America/Europe. This framework addresses the critical period when projected aerosol emission pathways diverge rapidly between high (SSP3-7.0) and low (SSP1-2.6) emission scenarios, with uncertainty in global aerosol emissions by 2050 comparable to (approximately 70% of) the total increase since 1850. The multi-model approach, requiring a minimum of 10-member ensembles from Coupled Model Intercomparison Project Phase 6 (CMIP6; Eyring *et al* 2016) generation Earth System Models, enables robust quantification of uncertainties and identification of model-dependent versus robust responses across the ensemble, and aids identification of forced responses compared to natural variability.

The specific aims of this study are to quantify how South Asian, East Asian, and global aerosol reductions affect the SASM through analysis of RAMIP experiments, and to understand the underlying mechanisms driving these responses. The remainder of this paper is structured as follows: section 2 describes the data and methods; section 3 presents model evaluation metrics demonstrating baseline monsoon simulation skill; section 4 presents results for pre-monsoon and monsoon season responses; and section 5 discusses implications and conclusions.

2. Data and methods

2.1. Observations

Four observational precipitation datasets are employed for validation of model performance over the South Asian domain during the historical period (1979–2014). The Asian Precipitation Highly-Resolved Observational Data Integration Towards Evaluation (APHRODITE; Yatagai *et al* 2012) provides gauge-interpolated precipitation analyses at 0.25° resolution specifically designed for Asian monsoon regions, drawing on an extensive network of daily rain-gauge records. The Global Precipitation Climatology Project (GPCP; Adler *et al* 2003) provides satellite-gauge merged precipitation estimates at 2.5° resolution; unlike the purely gauge-based products, GPCP blends GPCC gauge analyses with satellite-derived estimates that provide coverage where gauge density is low, including the Himalayan foothills and southern slopes. The Global Precipitation Climatology Centre (GPCC; Schneider *et al* 2014) provides a gauge-only global analysis at 0.5° resolution. We note that GPCP incorporates GPCC gauge data as one of its inputs; over the South Asian land domain both products are therefore substantially influenced by the same underlying gauge network. The India Meteorological Department (IMD) gridded daily precipitation dataset (Pai *et al* 2014) provides 0.25° resolution analyses over the Indian subcontinent based on 6955 rain-gauge stations; it is fully independent of GPCC and is widely regarded as the most reliable high-density observational product for the Indian land domain. Together the four datasets provide complementary estimates drawing on different methodologies and station networks. All purely gauge-based products (APHRODITE, GPCC, IMD) are subject to sparse gauge coverage above approximately 2000 m, which affects the reliability of estimates over the Himalayan foothills and elevated terrain; GPCP is less directly affected in these regions owing to its satellite component. Yatagai *et al* (2012) note that APHRODITE's algorithm reduces false penetration patterns seen in other gauge-based analyses, and that estimates over elevated regions differ between products due to gauge network differences.

2.2. RAMIP model experiments

This study utilises simulations from the RAMIP (Wilcox *et al* 2023), specifically focusing on Tier 1 coupled transient experiments spanning January 2015 to February 2051. The experimental framework employs a baseline-perturbation approach where the SSP3-7.0 scenario serves as the reference simulation against which regional aerosol emission modifications are compared. All experiments maintain identical greenhouse gas concentrations, land use changes, and natural emissions following the SSP3-7.0 pathway, ensuring that only the specified regional anthropogenic aerosol changes contribute to simulated climate differences between experiments. While some natural emissions (dust, sea salt, biogenic VOCs) are climate-dependent and may differ between experiments due to simulated climate changes, the experimental design minimises these differences by maintaining consistent SST and land surface forcing across experiments within each model.

The core experiments examined are the global aerosol reduction (ssp370-126aer) and regional reduction experiments: ssp370-EAS126aer (East Asia) and ssp370-SAS126aer (South Asia). In each perturbation experiment, anthropogenic aerosol and precursor emissions (SO_2, black carbon, and organic carbon) are modified to follow the SSP1-2.6 pathway within the specified geographical boundaries, while maintaining SSP3-7.0 emissions elsewhere. The South Asia region is defined as 5° N–35° N, 65° E–95° E, encompassing the core monsoon region and major emission sources including the IGP. The East Asia region is defined as 20° N–50° N, 100° E–145° E, covering the major industrial and population centres of China, the Korean Peninsula, and Japan.

Table 1. Model data citations and documentation references. Models used in monsoon season analysis are shown in **bold**; those used in pre-monsoon analysis are shown in *italics*. For more detailed information on aerosol and chemistry schemes across the RAMIP models, see Wilcox (2025).

Model	Institution	RAMIP data citation	Historical data citation	Model Doc.
CanESM5-1	CCCma, Canada	Fraser-Leach *et al* (2025)	Swart *et al* (2019b)	Swart *et al* (2019a)
CNRM-ESM2-1	CNRM-CERFACS, France	Nabat (2025)	Seferian (2018)	Séférian *et al* (2019)
GFDL-SPEAR_LO	NOAA/GFDL, USA	Paynter (2025)	NOAA Geophysical Fluid Dynamics (2020)	Delworth *et al* (2020)
MIROC6	MIROC, Japan	Takemura (2025)	Tatebe and Watanabe (2018)	Tatebe *et al* (2019)
NorESM2-LM	NCC, Norway	Lewinschal (2025)	Seland *et al* (2019)	Seland *et al* (2020)
CESM2	NCAR, USA	Allen (2025)	Danabasoglu (2019)	Danabasoglu *et al* (2020)
EC-Earth3-AerChem	EC-Earth Consortium	O'Donnell *et al* (2025)	EC-Earth-Consortium (2019)	van Noije *et al* (2021)
GISS-E2-1-G	NASA/GISS, USA	Westervelt *et al* (2025)	NASA/GISS (2018), Miller *et al* (2021)	Bauer *et al* (2020), Kelley *et al* (2020)
MRI-ESM2-0	MRI, Japan	Oshima and Koshiro (2025)	Yukimoto *et al* (2019b)	Yukimoto *et al* (2019a)
UKESM1-0-LL	MOHC, UK	Rumbold *et al* (2025)	Tang *et al* (2019)	Sellar *et al* (2019)

Table 2. Model technical specifications and aerosol schemes.

Model name	Atmospheric resolution	Aerosol scheme (type)	Levels	Model top
CanESM5-1	$2.8° \times 2.8°$ (128×64)	Interactive (bulk)	49	1 hPa
CNRM-ESM2-1	$1.4° \times 1.4°$ (256×128)	TACTIC v2 (modal)	91	78.4 km
GFDL-SPEAR_LO	$1.875° \times 1.875°$ (192×96)	AM4 aerosol (bulk)	33	1 hPa
MIROC6	$1.4° \times 1.4°$ (256×128)	SPRINTARS 6.0 (bulk)	81	0.004 hPa
NorESM2-LM	$1.9° \times 2.5°$ (144×96)	OsloAero (modal)	32	3 hPa
CESM2	$0.9° \times 1.25°$ (288×192)	MAM4 (modal)	32	2.25 hPa
EC-Earth3-AerChem	$0.7° \times 0.7°$ (512×256)	TM5 (bulk)	91	0.01 hPa
GISS-E2-1-G	$2° \times 2.5°$ (144×90)	OMA (bulk)	40	0.1 hPa
MRI-ESM2-0	$1.125° \times 1.125°$ (320×160)	MASINGAR mk2r4 (bulk)	80	0.01 hPa
UKESM1-0-LL	$1.875° \times 1.25°$ (192×144)	GLOMAP-mode (modal)	85	85 km

(type) denotes the aerosol size-distribution representation: *bulk* = bulk mass scheme (no explicit size distribution); *modal* = size distribution represented by prescribed log-normal modes.

Absorbing aerosols have previously been demonstrated to play an important role in monsoon dynamics, particularly during the pre-monsoon season through mechanisms such as the EHP. To isolate the specific impacts of absorbing aerosols, we also analyse the Tier 2 ssp370-SAS126ca experiment. In this experiment, only carbonaceous aerosol emissions (BC and OC) are perturbed within the South Asian domain, while all other aerosol species (including sulfates) and non-South Asian emissions follow SSP3-7.0. The difference between ssp370-SAS126ca and the baseline ssp370 experiment isolates the impact of local carbonaceous aerosol, which is critical for understanding elevated heating mechanisms given that black carbon acts as a warming agent in the atmosphere.

2.3. Model ensemble

The analysis is performed on a multi-model ensemble comprising ten CMIP6-generation Earth System Models participating in RAMIP: CanESM5-1, CNRM-ESM2-1, GFDL-SPEAR_LO, MIROC6, NorESM2-LM, CESM2, EC-Earth3-AerChem, GISS-E2-1-G, MRI-ESM2-0, and UKESM1-0-LL. This suite of models represents a diverse range of institutional contributors and model components, with varying levels of complexity in their representations of atmospheric physics, chemistry, and aerosol processes (see tables 1 and 2). The ensemble-mean historical (2014 vs 1850) effective radiative forcing due to aerosols is -1.06 ± 0.22 W m^{-2}, closely matching the CMIP6 multi-model mean of -1.12 W m^{-2}, with individual models spanning from -1.34 to -0.75 W m^{-2}. This range encompasses a substantial fraction of that seen in an analysis of the entire CMIP6 ensemble, ensuring our results are not biased toward models with unusually strong or weak aerosol forcing.

2.4. Analysis methods

The RAMIP experiments analysed in this study include ten ensemble members for each scenario, providing robust sampling of internal climate variability. Our analytical approach employs a comprehensive resampling methodology to quantify the climate response and associated uncertainties. All model data are regridded to a common grid (NorESM2-LM resolution: 1.9° × 2.5°, 144×96) using nearest-neighbour interpolation to facilitate multi-model analysis while preserving spatial features. For each variable and grid point, we calculate seasonal (JJA) averages for both the perturbation experiment and baseline scenario. We then implement an exhaustive pairwise comparison between all ensemble members, computing differences for every possible combination (e.g. $e_1 - b_1$, $e_2 - b_1$, $e_3 - b_1$, …, $e_1 - b_2$, $e_2 - b_2$, $e_3 - b_2$, …, where e represents ensemble members from the perturbation experiment and b represents those from the baseline scenario). This resampling approach, yielding 100 difference combinations for each experiment, provides robust statistical inference by utilising multiple iterations to assess the significance and agreement of projected changes. The multi-model JJA response maps (figures 5–7) are computed as 15 year means over 2036–2050. Because each experiment provides a 10-member ensemble, the pairwise differencing yields $10 \times 10 = 100$ realisations of the forced response per year, and 1500 over the 15 year window; internal variability is thereby suppressed by approximately $\sqrt{100} = 10$ relative to a single realisation. This is the rationale for the RAMIP requirement of a minimum of 10 ensemble members (Wilcox *et al* 2023): the concern that internal variability dominates a 15 year mean applies to single-realisation analyses rather than to the large pairwise ensemble used here.

Statistical significance of the climate response is assessed using a two-tailed t-test with a significance level of 0.10 (90% confidence level), applied independently at each grid point by comparing the distribution of differences against a null hypothesis of zero change. Model agreement is evaluated by calculating the proportion of ensemble member combinations agreeing on the sign of change, with robust agreement defined as at least 70% consensus (a lack of consensus is shown as hatching in spatial plots). For vector fields (moisture flux and winds), we calculate both magnitude changes and directional components. The moisture flux shown in panel (g) of figures 5–7 is the vertically integrated horizontal water-vapour transport,

$$\mathbf{Q} = \frac{1}{g}\int_{p_{\mathrm{sfc}}}^{300\,\mathrm{hPa}} q\,\mathbf{V}\,\mathrm{d}p, \tag{1}$$

where q is specific humidity (kg kg^{-1}), $\mathbf{V}$ the horizontal wind vector (m s^{-1}), g gravitational acceleration, and the integral runs from the surface to 300 hPa; the resulting unit kg m^{-1} s^{-1} is the standard unit used in atmospheric-river and monsoon moisture-transport studies.

Cross-sectional analyses of vertical velocity (omega) are performed for the ssp370-SAS126ca experiment to investigate the response of the EHP mechanism to carbonaceous aerosol reductions. The meridional (latitude–pressure) cross-sections (figures 2 and 3) average data over the 75–90° E core EHP longitudes to capture the circulation patterns that characterise the EHP response, while the 500 hPa spatial map (figure 4) covers 65–95° E. All of these analyses use a 15 year mean over 2036–2050, consistent with the JJA response maps and examining the period when the divergence between aerosol emission pathways is large. This period is consistent with the approach recommended in the RAMIP protocol (Wilcox *et al* 2023); pooling the full 2015–2050 period would conflate early years of small aerosol forcing differences with later years of large divergence, reducing rather than improving statistical robustness.

3. Model evaluation

Accurate simulation of the SASM remains a long-standing challenge in climate modelling, with persistent biases evident across multiple generations of coupled models (Sperber *et al* 2013). The South Asian monsoon exhibits particularly complex dynamics involving ocean-atmosphere-land interactions, orographic effects, and multiple tropical convergence zones, making it one of the most demanding systems to simulate. Previous model intercomparison studies have documented systematic biases in CMIP3 and CMIP5 models, including a general dry bias over the monsoon core region (particularly the IGP), excessive precipitation over surrounding oceans, and underestimation of the northwestward extension of the monsoon rainbelt (Sperber *et al* 2013).

Recent evaluations of CMIP6 models reveal systematic improvements in South Asian monsoon simulation compared to earlier generations, though significant biases persist (Choudhury *et al* 2022, Rajendran *et al* 2022, He *et al* 2023). The multi-model ensemble mean shows a reduced dry bias from −1.09 mm d^{-1} in CMIP3 to −0.70 mm d^{-1} in CMIP5 and −0.47 mm d^{-1} in CMIP6, alongside improved spatial pattern correlations and reduced root-mean-square errors (RMSE) (He *et al* 2023). Rajendran *et al* (2022) demonstrate that while systematic improvements are evident in simulating mean monsoon climatology, individual CMIP6 models show substantial spread in performance, with pattern correlations against observations ranging from 0.59 to 0.93. Despite these improvements, CMIP6 models still exhibit common deficiencies including wet biases over the equatorial Indian Ocean, cold SST biases in the northern Indian Ocean that weaken the upper-tropospheric thermal contrast, and underestimation of interannual variability (Rajendran *et al* 2022, He *et al* 2023). Models continue to struggle with accurately representing the narrow monsoon rainbelt extending northwestward from the Bay of Bengal across the IGP, which is critical for capturing interannual variability.

Model selection was based on spatial pattern performance (pattern correlation and RMSE). The annual cycle of all-India precipitation was additionally examined as a consistency check; both analyses are presented in the supplementary material (figures A1 and A2).

3.1. Validation methodology

Here, we employ spatial pattern correlation and RMSE metrics to quantify fidelity of the RAMIP models in reproducing observed June-July-August (JJA) precipitation climatology over South Asia. All observational data (APHRODITE, GPCP, GPCC, IMD) are regridded to a common grid (NorESM2-LM resolution: $1.9^\circ \times 2.5^\circ$, 144×96) using bilinear interpolation, which is appropriate for these spatially continuous point-measurement fields. Model output fields, by contrast, are cell-mean quantities and are regridded using nearest-neighbour interpolation to preserve original cell-mean values without introducing artificial spatial smoothing that would bias pattern correlation and RMSE metrics. Land-sea masks are applied based on APHRODITE data coverage to focus the analysis on terrestrial precipitation patterns. Ensemble statistics are calculated for each model to assess both mean performance and inter-model variability, with pattern correlations computed using area-weighted spatial fields to account for latitudinal convergence. This validation approach establishes the baseline representation of SASM precipitation in participating models, providing context for interpreting aerosol-induced changes in subsequent RAMIP experiments.

3.2. Model performance assessment

The CMIP6 models participating in RAMIP demonstrate varying levels of skill in reproducing observed South Asian monsoon precipitation patterns, with significant implications for confidence in projected aerosol impacts (figure 1; RMSE analysis in figure A2 of the supplementary material). The APHRODITE observational dataset provides a robust reference climatology for the historical period (1979–2014), exhibiting distinct precipitation maxima along the Western Ghats and northeastern India, well-defined orographic precipitation patterns, and the characteristic north-south gradient that defines the South Asian monsoon system.

Model performance assessment (figure 1) reveals a clear spread in pattern correlations across the ensemble, with the top third (pattern correlation > 0.8) including EC-Earth3-AerChem, which demonstrates the highest fidelity ($r = 0.93$), successfully capturing both the Western Ghats precipitation maximum and northeastern India rainfall patterns while maintaining the general north-south precipitation gradient. This superior performance is consistent with broader CMIP6 evaluations identifying EC-Earth3 variants among the top-performing models for South Asian monsoon simulation (Rajendran *et al* 2022, He *et al* 2023). CESM2 ($r = 0.84$), GFDL-SPEAR_LO ($r = 0.84$), CNRM-ESM2-1 ($r = 0.82$), and NorESM2-LM ($r = 0.82$) also demonstrate strong skill in reproducing these fundamental monsoon features, though with some regional intensity biases. These models consistently represent the spatial organisation of monsoon precipitation, including orographic enhancement over complex terrain. He *et al* (2023) similarly identify CNRM models among those showing stable performance across multiple monsoon characteristics, while Rajendran *et al* (2022) highlight MIROC6 and GFDL variants as exhibiting particularly good skill in simulating both mean monsoon patterns and coefficient of variation.

The middle third of the ensemble ($0.75 < r \leq 0.8$) includes MIROC6 ($r = 0.80$), UKESM1-0-LL ($r = 0.79$), and MRI-ESM2-0 ($r = 0.79$), which show reasonable pattern agreement with APHRODITE but exhibit some biases in the intensity and spatial extent of orographic precipitation. The bottom third ($r < 0.7$) consists of CanESM5-1 ($r = 0.63$) and GISS-E2-1-G ($r = 0.59$), which show notable systematic biases in the representation of orographic precipitation, overall rainfall intensity, and spatial distribution of precipitation maxima. These two models sit in a distinct cluster separated from the rest of the ensemble by a clear gap ($r = 0.59$–0.63 versus $r = 0.79$–0.93 for the remaining models).

The observational datasets demonstrate excellent internal consistency, with APHRODITE, IMD, GPCP, and GPCC showing pattern correlations exceeding 0.94. GPCP exhibits the strongest correlation

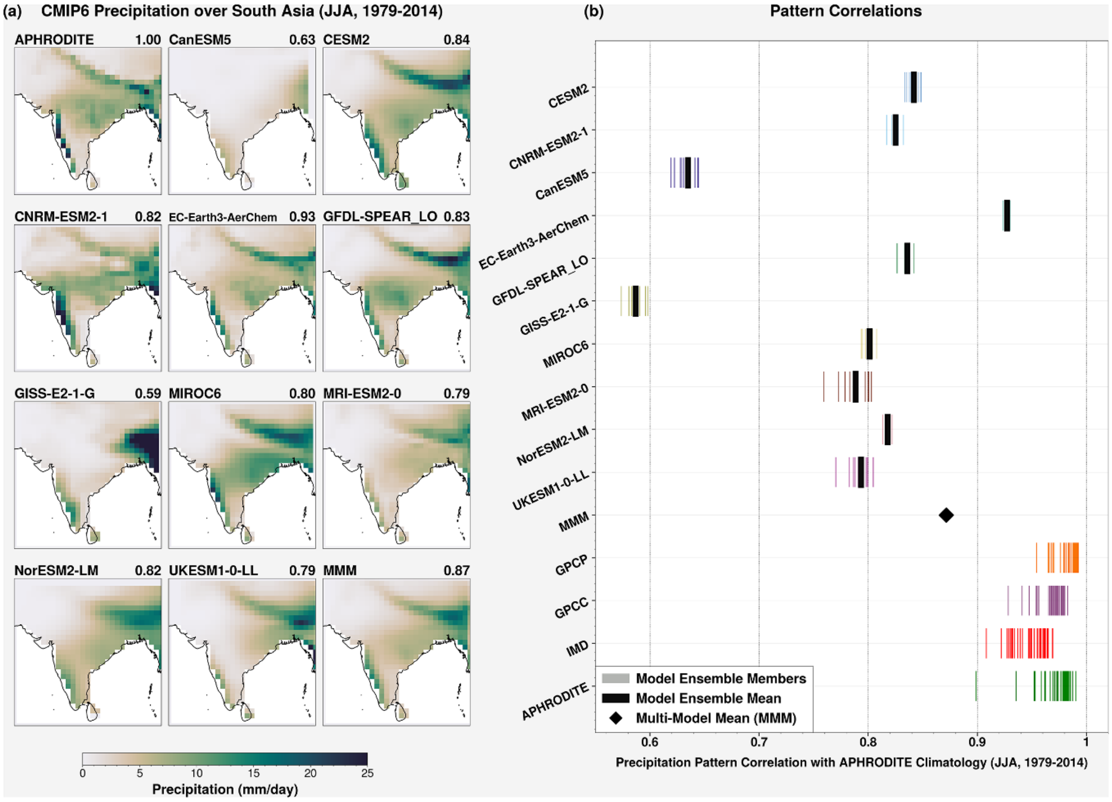

Figure 1. JJA precipitation climatology (1979–2014) over India (65–95°E, 5–35°N). (a) Spatial patterns of precipitation (mm d^{-1}) from APHRODITE observations (our baseline observational product) and RAMIP models. Numbers in the top right of each panel show pattern correlations with APHRODITE. (b) Pattern correlations with APHRODITE climatology (JJA, 1979–2014), showing individual years for observational datasets (GPCP, GPCC, IMD) and ensemble members for models (coloured lines for each model), along with ensemble means for models (black lines).

with APHRODITE ($r = 0.984$), reflecting the complementary nature of satellite and gauge-based precipitation estimates over the South Asian domain, while GPCC shows marginally lower correlation ($r = 0.969$), likely due to sparse gauge coverage over elevated Himalayan regions. For several models, the differences in pattern correlation between individual models and the observational reference are comparable in magnitude to the spread across the observational datasets themselves, and small inter-model differences in skill score should not be over-interpreted.

The top third by RMSE is represented by EC-Earth3-AerChem (RMSE = 1.46 mm d^{-1}), which demonstrates superior performance by successfully capturing both spatial patterns and precipitation magnitude with minimal systematic bias. The middle third (RMSE = 2.0–2.7 mm d^{-1}) includes GFDL-SPEAR_LO (2.21), NorESM2-LM (2.26), CESM2 (2.29), CNRM-ESM2-1 (2.34), MRI-ESM2-0 (2.42), UKESM1-0-LL (2.43), and MIROC6 (2.61 mm d^{-1}), showing reasonable representation of major precipitation features with moderate intensity biases. The bottom third comprises CanESM5-1 (3.51 mm d^{-1}) and GISS-E2-1-G (4.16 mm d^{-1}), with RMSE values roughly twice those of the other models (1.46–2.61 mm d^{-1}), exhibiting substantial systematic biases in precipitation intensity and spatial distribution.

Ensemble behaviour analysis reveals important characteristics of model representation of internal variability (figure A2b, supplementary material). Individual ensemble members (coloured lines) show relatively small spread for most models, with ensemble means (black lines) well-representing overall model behaviour. The inter-model spread significantly exceeds internal variability for most models, indicating that performance differences reflect structural differences rather than initialisation sensitivity. Small spread in ensemble members demonstrates that precipitation biases are primarily systematic rather than stochastic, with ensemble means generally representative of model behaviour. The clear separation between high and low performing models, combined with consistent relative performance across ensemble members, provides confidence that the RMSE analysis complements pattern correlation metrics effectively. This dual assessment reveals biases in monsoon intensity that are not captured by spatial correlations alone, establishing that models with strong spatial pattern correlation may still exhibit systematic intensity biases that could influence the magnitude of projected aerosol impacts.

Based on this evaluation, we identify two models with notably weaker performance than the others (CanESM5-1 and GISS-E2-1-G), which we exclude from the monsoon season multi-model mean analysis. Eight models demonstrating skill in reproducing observed South Asian monsoon precipitation patterns are selected for the primary multi-model mean analysis: CESM2, CNRM-ESM2-1, EC-Earth3-AerChem, GFDL-SPEAR_LO, MIROC6, MRI-ESM2-0, NorESM2-LM, and UKESM1-0-LL. The performance hierarchy identified through this validation analysis (described in section 3) provides essential context for interpreting aerosol-induced precipitation changes in subsequent RAMIP experiments, with higher confidence placed on results from models demonstrating superior baseline monsoon simulation skill. The annual cycle of all-India precipitation for all ten models is shown in figure A1 of the supplementary material, providing additional support for the exclusion of CanESM5-1 and GISS-E2-1-G; the RMSE analysis is shown in figure A2.

4. Results

Pre-monsoon aerosol-circulation interactions operate through fundamentally different mechanisms than those during the established monsoon season, with absorbing aerosols playing a particularly important role through the EHP mechanism. To understand how regional aerosol reductions affect the SASM, we first examine pre-monsoon EHP responses (section 4.1) using two models that provided carbonaceous aerosol perturbation experiments, then examine the monsoon season responses (JJA) to South Asian (section 4.2), global (section 4.3), and East Asian (section 4.4) aerosol reductions using the multi-model ensemble mean from the eight best-performing models (identified in section 3).

4.1. Pre-Monsoon circulation response to carbonaceous aerosol reductions

During the pre-monsoon season (March–May), the South Asian region experiences the development of the EHP mechanism, characterised by strong mid-tropospheric ascent over the IGP extending to the Himalayan foothills and Tibetan Plateau. This circulation pattern, evident in the baseline ssp370 climatology, shows intense upward motion concentrated along the Himalayan arc from 75°E to 90°E. The EHP mechanism is driven by absorbing aerosol-induced atmospheric heating that creates a thermally-direct circulation, transporting energy from the IGP to elevated layers where it enhances convective activity over orographically complex terrain. The seasonal evolution intensifies from March through May, with maximum upward motion occurring during May as absorbing aerosol concentrations peak and solar radiation strengthens prior to monsoon onset.

The meridional cross-sections of vertical velocity over the IGP reveal distinct modifications to the EHP mechanism when carbonaceous aerosol emissions are reduced in South Asia (figure 2). We present results from MIROC6 and CNRM-ESM2-1 because they were the only two models that provided Tier 2 simulations and had good performance in simulating SASM as representatives of the model response; while the individual models show variations in spatial details and magnitude due to differences in their baseline climatologies and aerosol parametrisations, both demonstrate consistent weakening of the EHP circulation pattern in response to carbonaceous aerosol reductions.

MIROC6: The climatological vertical velocity field (shaded) for the baseline ssp370 scenario shows the characteristic pre-monsoon circulation pattern, with strong upward motion extending over the Himalayan foothills (28°N–35°N) intensifying from March through May, reaching maximum intensities exceeding -40 hPa d^{-1} at mid-tropospheric levels (400–600 hPa). The response to carbonaceous aerosol reductions (ssp370-SAS126ca minus ssp370, shown as line contours) demonstrates a systematic weakening of the elevated heating mechanism across all pre-monsoon months. In March, the response is relatively modest, with positive anomalies (dashed lines) of $+0.8$ to $+1.6$ hPa d^{-1} appearing around 25–30°N at mid-tropospheric levels (400–600 hPa), indicating the initial stages of EHP weakening when climatological upward motion is typically developing. This pattern intensifies through April, with positive anomalies strengthening to $+1.6$ to $+3.2$ hPa d^{-1} and expanding vertically through the mid-troposphere, particularly over the Himalayan foothills (28–32°N). The spatial organisation becomes more coherent in April, with the positive anomalies clearly aligned with regions of climatologically strong upward motion.

Crucially, the temperature rows of figure 2 supply the thermodynamic evidence underlying this circulation change, demonstrating the EHP through temperature rather than vertical velocity alone. Reducing carbonaceous aerosol removes a source of mid- and upper-tropospheric radiative heating, producing a predominantly negative air-temperature anomaly (reaching up to -0.4 K in MIROC6 and CNRM-ESM2-1) through the mid-troposphere over the Himalayan foothills (28–35°N). This cooling aloft is co-located, month by month, with the positive (weakening) vertical-velocity anomaly: the latitudes and months of

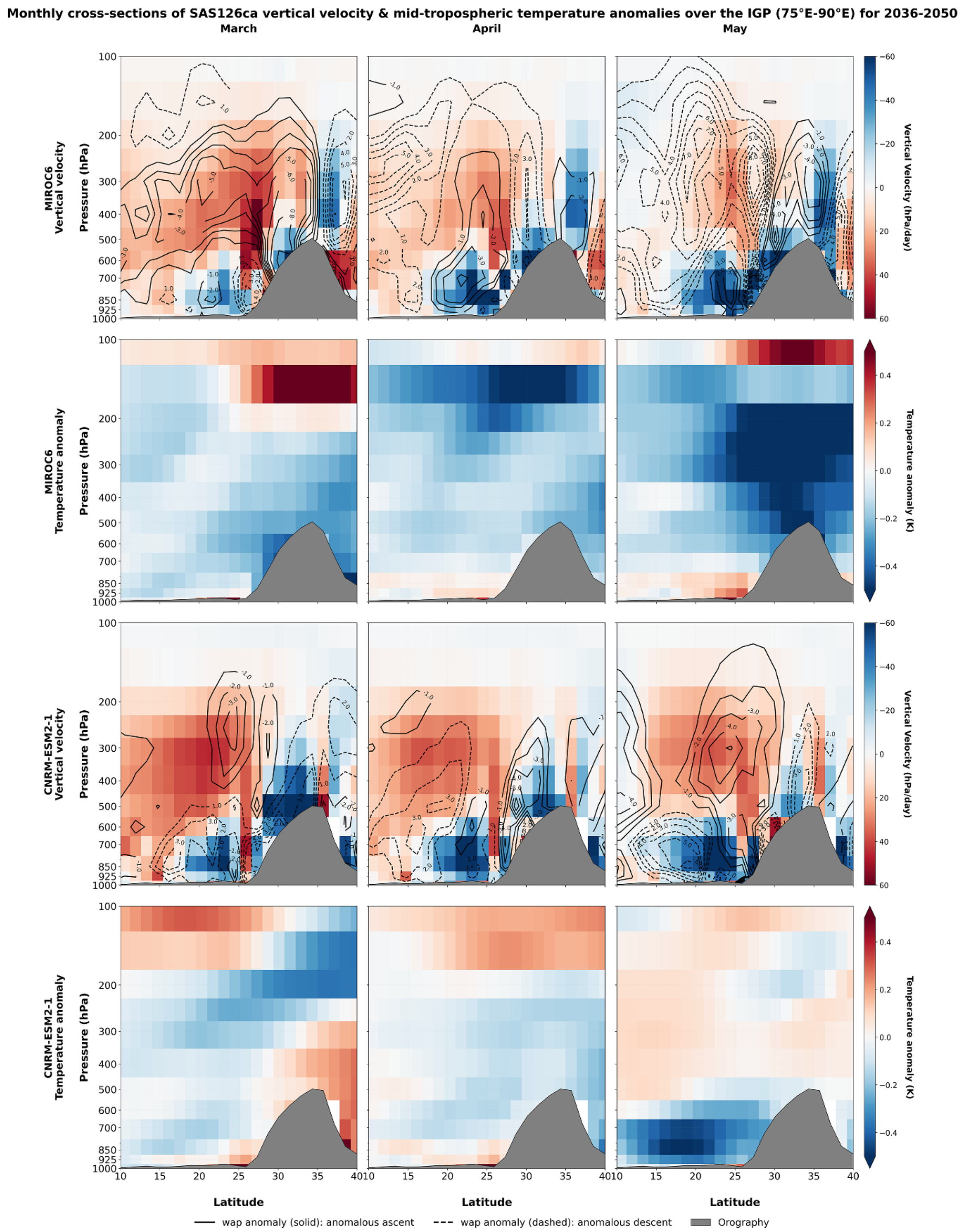

Figure 2. Monthly meridional cross-sections (latitude–pressure, averaged over 75–90° E) of the carbonaceous-aerosol response (ssp370-SAS126ca minus ssp370) for MIROC6 and CNRM-ESM2-1 (ensemble means, 2036–2050). For each model the upper row shows vertical velocity (climatology shaded, hPa d^{-1}, blue ascent / red descent; anomalies as contours, solid = anomalous ascent, dashed = anomalous descent) and the lower row shows the air-temperature anomaly (shaded, (K). Columns are March, April and May. Grey shading represents orography.

strongest mid-tropospheric cooling coincide with those of strongest reduction in climatological ascent, with the cooling strongest in MIROC6 in May; CNRM-ESM2-1 shows the same sense of response but closer to the foothills. The temperature anomaly thus identifies the reduced elevated heating as the cause and the weakened ascent as its dynamical consequence, completing the demonstration of EHP weakening in the sense intended by Lau and Kim (2006).

May exhibits the most dramatic EHP disruption for MIROC6, with extensive positive anomalies reaching +2.4 to +5.0 hPa d^{-1} concentrated over the Himalayan region (28–35°N) between 400–600 hPa. These anomalies due to local reductions in carbonaceous aerosol directly counteract the climatological upward motion that peaks during May (exceeding -40 hPa d^{-1} in the baseline), representing a substantial weakening of the EHP's core mechanism. Quantified over the Himalayan foothills box (28–35°N, 400–600 hPa, 75–90°E), the carbonaceous-aerosol reduction cools the mid-troposphere by up to 0.4 K in MIROC6 (box-mean anomalies of -0.29, -0.14 and -0.41 K in March, April and May) and drives localised anomalous descent of up to $+9.6$ hPa d^{-1} that directly opposes the climatological ascent. Because anomalous ascent and descent cells occur side by side within the box, the box-averaged vertical-velocity change is small and spatially variable; the robust, coherent signature of EHP weakening is therefore the mid-tropospheric cooling, a smoother diagnostic than the low-amplitude vertical-velocity field. The vertical structure of these positive anomalies extends from the lower troposphere (700 hPa) through the mid-troposphere (400 hPa), indicating that the reduction in black carbon heating affects multiple atmospheric layers where absorbing aerosols typically exert maximum radiative effects. Some regions show weak negative anomalies (solid contours) at lower latitudes (15–25°N), suggesting localised weakening of climatological descent, though these are substantially weaker than the dominant positive anomalies over the Himalayan region.

CNRM-ESM2-1: This model demonstrates broadly consistent EHP weakening but with distinctive characteristics reflecting its different model physics and higher vertical resolution (figure 2, bottom row). March shows the baseline circulation with intense mid-tropospheric upward motion (exceeding -50 hPa d^{-1}, stronger than MIROC6) around 250–500 hPa at 25–35°N, with weak positive anomalies ($+1.0$ hPa d^{-1}) appearing around 30–35°N indicating initial EHP weakening. April exhibits a complex heterogeneous pattern with both positive anomalies (dashed, $+1.0$ to $+3.0$ hPa d^{-1}) at various latitudes and some weak negative anomalies at lower levels. May shows EHP weakening with positive anomalies ($+2.0$ to $+4.0$ hPa d^{-1}) concentrated around 30–35°N at mid-tropospheric levels, overlaying regions of strong climatological upward motion (exceeding -40 hPa d^{-1}). The response in CNRM-ESM2-1 is more vertically confined than in MIROC6, with maximum anomalies focused around 400–500 hPa rather than extending through a broader vertical column. This difference may reflect the higher vertical resolution in CNRM-ESM2-1 and/or differences in the vertical distribution of aerosol mass mixing ratios between the two models. Despite these structural differences, both models demonstrate the fundamental EHP weakening mechanism, with positive anomalies opposing climatological upward motion over the Himalayan region during the critical pre-monsoon months. The consistency of this response across models with very different atmospheric physics, vertical resolution, and convection schemes provides confidence in the robustness of local carbonaceous aerosol control over pre-monsoon circulation.

Comparison with the full aerosol reduction experiment (figure 3) for MIROC6 reveals qualitatively similar EHP weakening but with somewhat different characteristics. The ssp370-SAS126aer response shows positive anomalies of similar spatial structure but generally weaker magnitude, particularly in April and May, suggesting that the simultaneous reduction of sulfate aerosols partially offsets the EHP weakening through increased surface heating and altered atmospheric stability. The vertical structure remains similar, with mid-tropospheric positive anomalies dominating, but the response is more spatially diffuse. This comparison confirms that absorbing aerosols are the primary driver of the EHP mechanism, while scattering aerosols modulate but do not eliminate the EHP response. The geographic contrast in figure 3 confirms the local origin of the EHP response: the South Asian experiments produce their strongest anomalies over the Himalayan foothills, whereas the East Asian experiment produces comparable anomalies at lower latitudes (15–25°N) rather than over the foothills, the characteristic signature of a Walker-circulation teleconnection rather than a local EHP response.

In striking contrast, the East Asian aerosol reduction experiment (ssp370-EAS126aer) for MIROC6 shows minimal systematic influence on South Asian pre-monsoon circulation (figure 3, middle row), consistent with findings by Herbert *et al* (2021). March exhibits very weak and spatially scattered anomalies over the IGP region, with small positive contours ($+0.4$ to $+0.8$ hPa d^{-1}) lacking spatial coherence or systematic alignment with climatological circulation features. April shows a more complex pattern with both negative anomalies indicating enhanced upward motion in some locations around 28–35°N, and positive anomalies elsewhere, but without the systematic structure observed in the South Asian experiments. May continues this pattern of spatial heterogeneity, with strong negative anomalies (-1.6 hPa d^{-1}) appearing around 30–35°N alongside positive anomalies in other regions, creating a complex patchwork that lacks the coherent EHP weakening signal. Statistical significance testing would be useful to determine which of these features represent robust responses versus internal variability.

The fundamental difference between the South Asian and East Asian aerosol experiments confirms that the pre-monsoon EHP mechanism over South Asia is controlled by local absorbing aerosol heating rather than remote influences. While East Asian aerosol reductions create substantial heating changes over East Asia and the northern Tibetan Plateau, these changes do not systematically modify the South Asian EHP circulation pattern during March–May. The mixed signals and spatial heterogeneity in the

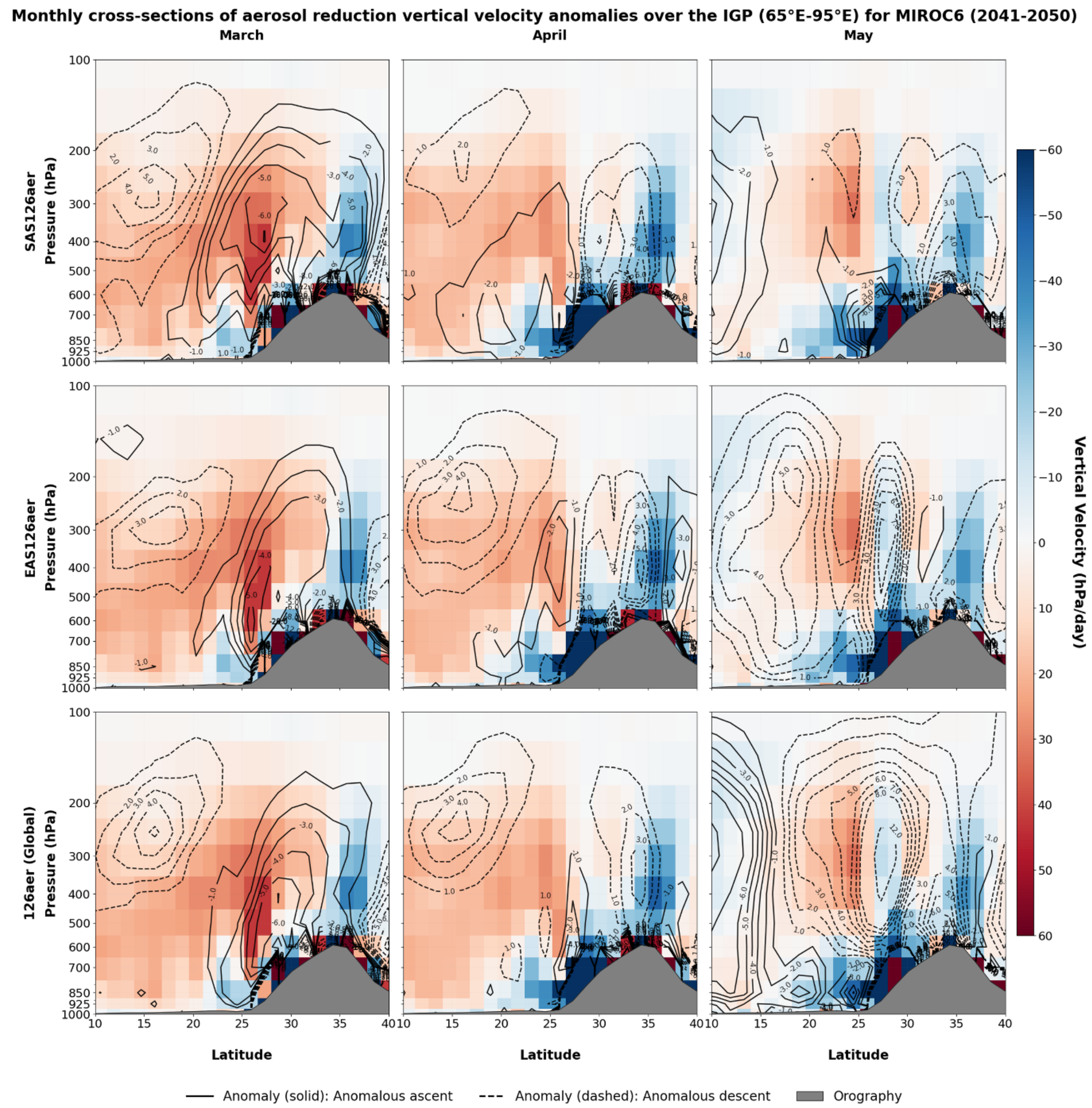

Figure 3. Monthly cross-sections of vertical velocity climatology (shaded, hPa d^{-1}, where blue represents ascent and red represents descent) and anomalies (contours, hPa d^{-1}) over the IGP ($75° 10^{-90°}$ E) for MIROC6 (2036–2050) across three aerosol reduction experiments. Top row: South Asian aerosol reduction (ssp370-SAS126aer minus ssp370). Middle row: East Asian aerosol reduction (ssp370-EAS126aer minus ssp370). Bottom row: Global aerosol reduction (ssp370–126aer minus ssp370). The climatology is based on ssp370. Solid contours indicate anomalous ascent (negative omega anomalies), while dashed contours represent anomalous descent (positive omega anomalies).

EAS126aer response suggest that remote aerosol forcing may induce some local circulation adjustments, but these do not project coherently onto the organised EHP structure. This finding aligns with the physical understanding that the EHP requires co-location of absorbing aerosol heating with orographic features to generate the thermally-direct circulation, a condition satisfied only by local South Asian aerosols during the pre-monsoon season (Lau *et al* 2006, Vinoj *et al* 2014).

The global aerosol reduction experiment (ssp370-126aer) for MIROC6 exhibits a pre-monsoon response over South Asia that reflects primarily the local South Asian forcing component (figure 3, bottom row), though with additional complexity. March shows relatively weak and spatially heterogeneous anomalies similar to but slightly stronger than the EAS experiment, while April demonstrates clearer positive anomalies over the Himalayan region, indicating EHP weakening consistent with the South Asian experiments but of intermediate magnitude. May exhibits strong variability with positive anomalies appearing at both circulation climatologies, suggesting that the combination of local South Asian and remote forcing introduces additional complexity to the circulation response. The overall pattern confirms that while global aerosol distributions modulate the response magnitude and spatial pattern, local South Asian absorbing aerosols remain the dominant driver of pre-monsoon EHP dynamics.

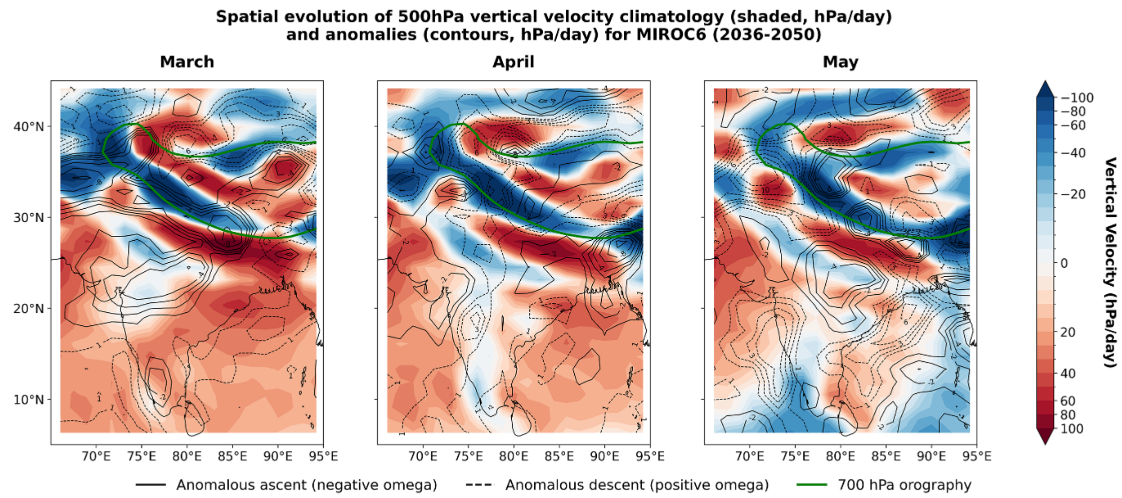

Figure 4. Spatial evolution of 500 hPa vertical velocity climatology (shaded, hPa d^{-1}, where red represents ascent and blue represents descent) and anomalies (contours, hPa d^{-1}) over the IGP ($65^\circ 10^{-95^\circ}$ E) for MIROC6 (2036–2050). The climatology is based on ssp370, while anomalies show the difference between ssp370-SAS126ca and ssp370. For the anomalies, solid contours indicate anomalous ascent (negative values), while dashed contours represent anomalous descent (positive values). The green line represents the 700 hPa orography.

The spatial evolution of 500 hPa vertical velocity for MIROC6 reveals how carbonaceous aerosol reductions systematically disrupt the established mid-tropospheric circulation patterns across the Indian subcontinent in the pre-monsoon period (figure 4). The baseline climatology establishes the pre-monsoon circulation context, showing characteristic intense upward motion (-30 to -60 hPa d^{-1}) concentrated along the Himalayan arc and extending over the Tibetan Plateau, representing the EHP's normal operation. When carbonaceous aerosols are reduced, a clear pattern emerges of weakened circulation precisely where the climatological upward motion is strongest.

In March, the response shows initial disruption of the EHP mechanism, with positive anomalies beginning to develop over the Himalayan foothills. Over the IGP, where climatological circulation is more modest, the anomaly patterns create alternating zones that fragment the coherent northward flow of the heat pump mechanism. By April, the disruption becomes more systematically organised across distinct Indian regional domains. The most pronounced changes occur where climatological upward motion is strongest: along the Himalayan foothills from Himachal Pradesh to Uttarakhand and extending into Nepal. Here, positive anomalies ($+1.6$ to $+2.4$ hPa d^{-1}) directly counteract the climatological upward motion (-40 to -60 hPa d^{-1}), representing a fundamental weakening of the mid-tropospheric ascent. The southern peninsular regions, where climatological circulation is less intense, show correspondingly smaller anomaly responses, confirming the regional specificity of elevated heating effects.

The May pattern demonstrates the most dramatic reorganisation, with extensive positive anomalies ($+2.0$ to $+4.0$ hPa d^{-1}) developing precisely over areas where the climatology exhibits maximum upward motion intensity. The entire Himalayan arc, from the western mountains of Kashmir through the central peaks of Nepal to the eastern ranges of Bhutan, shows strong positive anomalies superimposed on climatological upward motion exceeding -50 hPa d^{-1}. This represents a systematic suppression of the EHP's core mechanism. Northwestern India, where climatological upward motion is sustained and moderate (-20 to -40 hPa d^{-1}), shows positive anomalies indicating systematic weakening throughout the pre-monsoon season. Central India experiences more complex responses because climatological circulation is weaker and more variable, leading to spatially heterogeneous anomaly patterns. The progressive intensification of positive anomalies from March through May, concentrated over regions of maximum climatological upward motion, reveals how reduced black carbon heating systematically dismantles the mid-tropospheric circulation architecture that supports pre-monsoon energy transport from the IGP to elevated Himalayan layers.

4.2. Summer monsoon response to south Asian aerosol reductions

Shifting from pre-monsoon to the established monsoon season JJA, we now examine multi-model responses from the eight best-performing models (section 3 and table 1) for the South Asian aerosol reduction experiment (ssp370-SAS126aer).

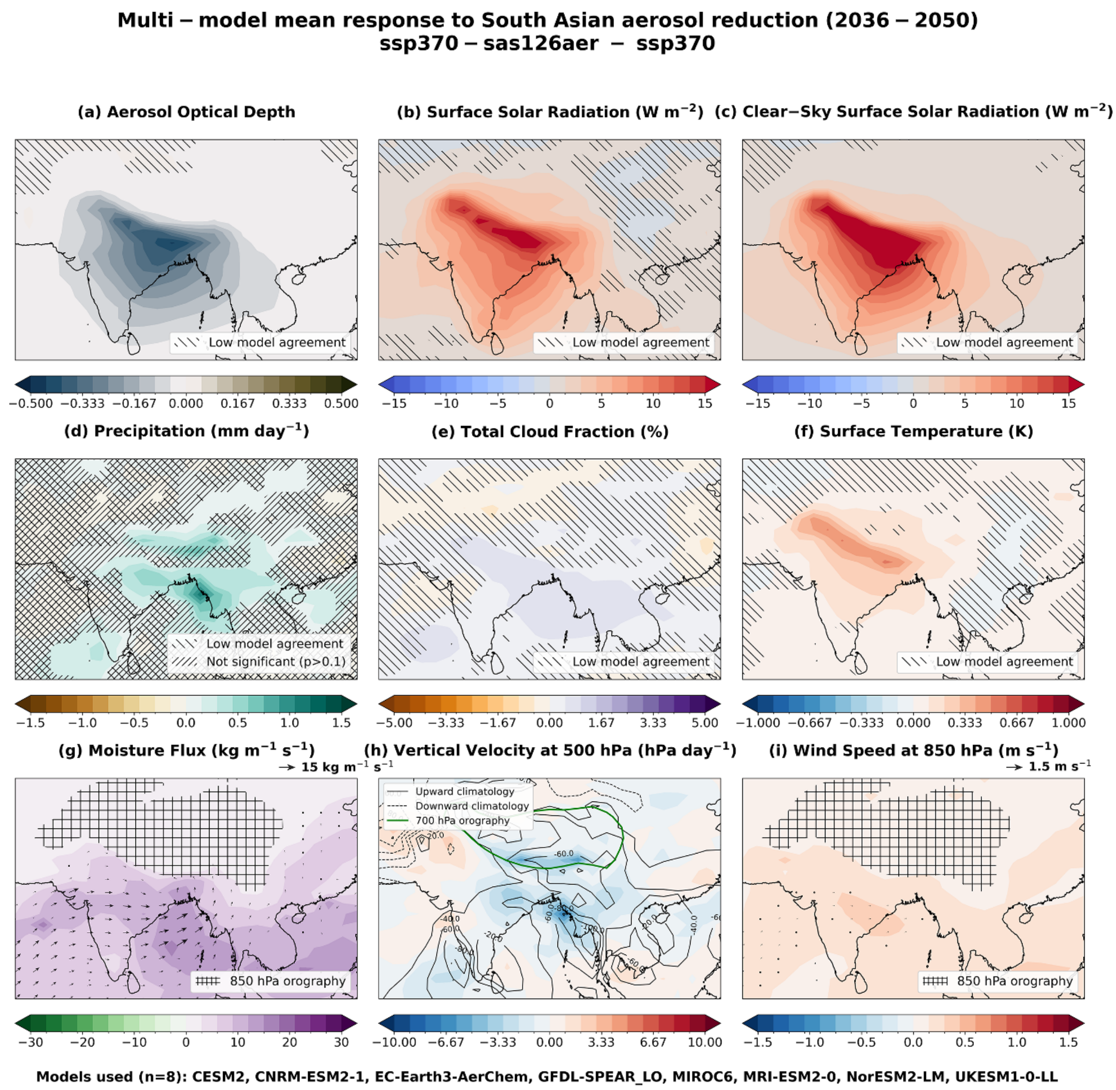

Figure 5. Multi-model mean response to South Asian aerosol reduction (ssp370-SAS126aer minus ssp370) for June-July-August 2036–2050: (a) aerosol optical depth, (b) downwelling shortwave radiation at the surface [$\mathrm{W\,m^{-2}}$], (c) downwelling shortwave radiation at the surface (clear-sky) [$\mathrm{W\,m^{-2}}$], (d) precipitation [$\mathrm{mm\,d^{-1}}$], (e) total cloud fraction, (f) surface temperature [K], (g) vertically integrated horizontal moisture flux [$\mathrm{kg\,m^{-1}\,s^{-1}}$], (h) vertical velocity at 500 hPa [$\mathrm{hPa\,d^{-1}}$], (i) wind speed at 850 hPa [$\mathrm{m\,s^{-1}}$]. Regions without hatching show where at least 70% of models agree on sign of change.

The climate response to South Asian aerosol reductions reveals strong local enhancement of the SASM through multiple interconnected mechanisms (figure 5). The reduction in AOD over the IGP and broader South Asian domain drives a cascade of radiative and dynamical responses that fundamentally alter regional hydroclimate patterns. The AOD decrease of 0.2–0.4 represents a substantial reduction in atmospheric aerosol loading, comparable in magnitude but opposite in sign to historical aerosol increases over this region since the 1950 s (Dey and Di Girolamo 2011).

Surface solar radiation increases by 10–15 $\mathrm{W\,m^{-2}}$ across the Indian subcontinent, with maximum enhancement over the IGP where baseline aerosol concentrations, and subsequent reductions, are highest. This direct radiative effect is pronounced in clear-sky conditions, though aerosol-radiation interactions dominate the all-sky signal, as confirmed by comparison between clear-sky and all-sky panels. Averaged over the analysis domain (60–120°E, 5–40°N), the clear-sky and all-sky shortwave increases are nearly identical (+3.6 versus +3.1 $\mathrm{W\,m^{-2}}$; locally up to +22 and +17 $\mathrm{W\,m^{-2}}$ respectively), so the cloud offset is only ∼15% of the clear-sky gain. The surface brightening is therefore overwhelmingly the direct clear-sky aerosol effect rather than a cloud response, and is not radiatively tied to the precipitation increase. Over the monsoon region the deep convective clouds in fact exert a net shortwave cooling at the surface, their shortwave cloud radiative effect exceeding the longwave (Rajeevan and Srinivasan 2000), so the increased convective cloudiness accompanying the rainfall response would reduce surface shortwave, reinforcing that the brightening is the direct aerosol effect. The enhanced shortwave reaching the surface drives temperature increases of up to +0.3 K averaged over the IGP core region (72–82°E, 24–28°N) in the multi-model mean, with the strongest warming occurring over the IGP matching the AOD and shortwave anomaly patterns. These temperature responses show excellent model agreement, indicating robust consensus across the multi-model ensemble about the magnitude and spatial pattern of surface warming. Importantly, the warming tracks the shortwave anomaly rather than the precipitation: the domain area-mean surface-temperature anomaly is markedly weaker over the heavy-rain cells than over the high-radiation cells (+0.09 versus +0.17 K). Surface warming and the precipitation increase are therefore not co-located (panels (f) and (g)), so the climatological inverse rainfall–temperature relationship (in which local rainfall cools the surface through latent-heat exchange; Trenberth and Shea 2005) does not apply to this aerosol-forced response: here the land warms relative to the ocean, strengthening the meridional tropospheric temperature gradient that—rather than the local surface temperature—dynamically drives the circulation (Goswami and Chakravorty 2017, Gadgil 2018), while the resulting rainfall maximises elsewhere.

Precipitation responses demonstrate robust enhancement across parts of South Asia, with a multi-model mean all-India increase of +0.19 mm d^{-1}. Regional responses are largest over the northern Bay of Bengal (area-mean +0.56, local peak +1.14 mm d^{-1}, with high model agreement), north-east India (area-mean +0.38, peak +0.70 mm d^{-1}), the IGP (area-mean +0.20, peak +0.51 mm d^{-1}) and central India (area-mean +0.16, peak +0.40 mm d^{-1}), while the Western Ghats shows a more modest response (area-mean +0.06, peak +0.17 mm d^{-1}) with lower model agreement. These increases scale with the local aerosol reduction: the JJA AOD decrease of 0.2–0.3 over the IGP and northern Bay of Bengal accompanies local precipitation increases peaking at +0.5 and +1.1 mm d^{-1} respectively, a regional sensitivity of order 2–5 mm d^{-1} per unit AOD. The spatial pattern of precipitation enhancement closely follows the climatological monsoon rainfall distribution (see figure 1), with maximum increases occurring along established monsoon pathways including the Western Ghats orographic rainfall region (where climatological precipitation exceeds 15 mm d^{-1}) and the monsoon trough extending across central India and the IGP (climatological values of 8–12 mm d^{-1}). This correspondence indicates that aerosol reductions primarily intensify the existing monsoon circulation pattern rather than fundamentally altering its spatial structure.

The eight best-performing models identified through our evaluation (section 3 and table 1) demonstrate precipitation responses that are generally consistent with the full ensemble, though with slightly enhanced magnitude over the core monsoon regions. These eight models show a more consistent response in area-mean precipitation changes over northern Bay of Bengal with a multi-model mean of +0.56 mm d^{-1} (range +0.28 to +0.82 mm d^{-1}). (The two excluded models, CanESM5-1 and GISS-E2-1-G, have very little baseline precipitation, so their absolute changes are proportionally smaller; see section 3). Without normalising by baseline precipitation or evaporation, we do not interpret the larger absolute responses of the higher-skill models as indicating greater sensitivity to aerosol forcing.

The moisture flux analysis reveals intensified low-level moisture transport from the Arabian Sea, with vectors showing strengthened south-westerly flow that enhances moisture convergence over the Indian peninsula. The magnitude of this intensification (5–10 kg m^{-1} s^{-1} anomalies) is substantial relative to the climatological moisture flux, representing a 10%–15% enhancement of the baseline monsoon circulation. This intensification of the monsoon circulation is consistent with the thermal gradient mechanism, where reduced aerosol loading enhances the land-sea temperature contrast that drives monsoonal flow.

The 500 hPa vertical velocity field shows enhanced upward motion over the monsoon trough region, with a multi-model mean anomaly of approximately −1.3 hPa d^{-1} over the core ascent region (75–85°E, 18–26°N). The strengthening of mid-tropospheric ascent over central India, combined with enhanced subsidence over the northern Arabian Sea, reflects an intensification of the regional Hadley circulation associated with stronger monsoon circulation (Wang *et al* 2021). Consistent but modest cloud fraction increases accompany the enhanced convection, providing a positive feedback through increased atmospheric moisture retention and latent heat release.

4.3. Summer monsoon response to global aerosol reductions

The global aerosol reduction experiment (ssp370-126aer) examines the combined effect of worldwide emission reductions on the South Asian monsoon using the multi-model mean from eight best-performing models.

Global aerosol reductions amplify and extend the regional responses observed from South Asian emission changes alone, while introducing additional large-scale dynamical adjustments that fundamentally alter monsoon behaviour (figure 6). The worldwide reduction in aerosol emissions creates a more homogeneous response within the Northern Hemisphere, where most anthropogenic aerosol emissions are concentrated. This Northern Hemisphere-dominant forcing pattern influences inter-hemispheric energy transport and tropical circulation patterns, particularly through modifications to the position and

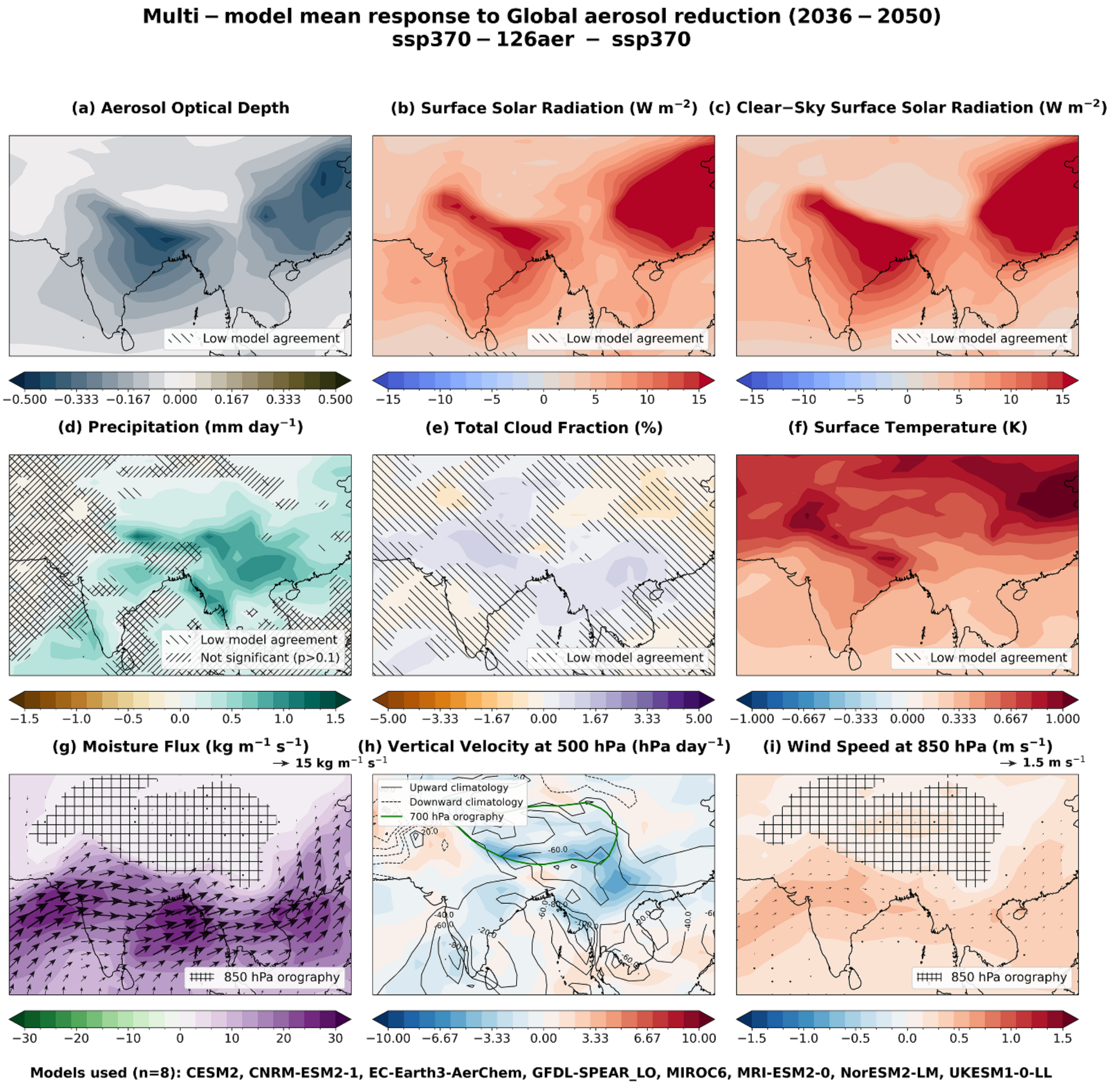

Figure 6. Multi-model mean response to global aerosol reduction (ssp370-126aer minus ssp370) for June-July-August 2036–2050: (a) aerosol optical depth, (b) downwelling shortwave radiation at the surface [W m^{-2}], (c) downwelling shortwave radiation at the surface (clear-sky) [W m^{-2}], (d) precipitation [mm d^{-1}], (e) total cloud fraction, (f) surface temperature [K], (g) vertically integrated horizontal moisture flux [kg m^{-1} s^{-1}], (h) vertical velocity at 500 hPa [hPa d^{-1}], (i) wind speed at 850 hPa [m s^{-1}]. Regions without hatching show where at least 70% of models agree on sign of change.

intensity of the Intertropical Convergence Zone (ITCZ). The global AOD reduction shows pronounced decreases over all major emission regions (figure 6(a)), with the largest changes over East and South Asia where current emissions are highest, creating a more zonally uniform forcing pattern compared to the regional experiments.

Surface solar radiation increases globally by 5–15 W m^{-2} (figure 6(b)), with particularly strong enhancement over the Northern Hemisphere continents where anthropogenic aerosol loadings are concentrated. This asymmetric heating pattern between hemispheres drives fundamental changes in the global energy budget and meridional energy transport (Hwang *et al* 2013). Critically, since most aerosol emission reductions occur in the Northern Hemisphere (particularly East and South Asia, with smaller contributions from North America and Europe), the preferential Northern Hemisphere warming reduces the inter-hemispheric temperature gradient and shifts the ITCZ northward (Shawki *et al* 2018). The clear-sky radiation changes over South Asia (figure 6(c)) show patterns similar to all-sky conditions, though the global response exhibits stronger contributions from thermodynamical and dynamical cloud adjustments and cloud feedbacks (rather than solely microphysical aerosol-cloud interactions) compared to the regional South Asian experiment, as evidenced by the larger difference between clear-sky and all-sky forcing over oceanic regions where marine stratocumulus clouds are prevalent. Surface temperature increases of 0.5–1.0 K occur across most land regions (figure 6(f)), with model agreement particularly robust over South Asia and East Asia, where aerosol reductions are largest. Over the analysis domain the clear-sky and all-sky shortwave increases are again essentially equal (+8.10 versus +8.04 W m^{-2}; cloud offset ∼1%), confirming that the surface brightening is the direct aerosol radiative effect. The causal sequence is therefore: reduced aerosol → increased clear-sky shortwave at the surface → land warming → strengthened moisture flux and convection → enhanced precipitation. Because these steps are not spatially coincident, increased surface radiation and increased rainfall coexist over South Asia without contradiction.

The precipitation response to global aerosol reductions (figure 6(d)) shows widespread increases across the Northern Hemisphere tropics and subtropics, with the South Asian monsoon region experiencing a multi-model mean all-India increase of +0.28 $mm\,d^{-1}$, with regional responses peaking over the IGP (area-mean +0.36, local peak +1.23 $mm\,d^{-1}$), the northern Bay of Bengal (area-mean +0.45, peak +0.98 $mm\,d^{-1}$) and central India (area-mean +0.32, peak +0.59 $mm\,d^{-1}$); the AOD decrease of ∼0.3 over the IGP accompanies the +1.2 $mm\,d^{-1}$ peak, a sensitivity of ∼5 $mm\,d^{-1}$ per unit AOD. This response exceeds that from regional South Asian reductions alone by approximately 45%, indicating important contributions from remote aerosol changes and large-scale circulation adjustments. The enhanced precipitation not only intensifies along traditional monsoon regions of Western Ghats and IGP but also extends spatially into the northern Bay of Bengal and eastern India, suggesting a northward and eastward expansion of the monsoon domain. This pattern is consistent with theoretical expectations of ITCZ shifts in response to inter-hemispheric heating asymmetries (Chung and Soden 2017, Wang *et al* 2019).

Model agreement on these precipitation responses (figure 6(d)) is notably stronger (larger areas without hatching) in the global experiment compared to the regional South Asian experiment, particularly over oceanic regions of the tropical Indian Ocean and western Pacific. This enhanced consensus reflects the larger signal-to-noise ratio when aerosol reductions occur globally rather than regionally, and suggests that the large-scale ITCZ response is a more robustly simulated feature than regional circulation adjustments. However, over land regions of central India, model spread remains substantial (presence of hatching), likely reflecting persistent differences in how models represent land-atmosphere coupling and convective organisation.

The moisture flux patterns (figure 6(g)) reveal a fundamental reorganisation of tropical moisture transport, with enhanced convergence over South Asia driven by both strengthened local monsoon circulation and northward-shifted tropical convergence. The intensified moisture transport from the tropical Indian Ocean combines with enhanced cross-equatorial flow to create more favourable conditions for deep convection over the monsoon region. The 500 hPa vertical velocity (figure 6(h)) shows widespread enhancement of upward motion across the Asian monsoon domain, with a northward broadening of the ascent zone consistent with reduced inter-hemispheric temperature gradients (Broccoli *et al* 2006). This northward expansion of the ascending branch of the monsoon Hadley cell represents a key mechanism by which global aerosol reductions amplify South Asian monsoon precipitation beyond what local emission changes alone would produce.

Cloud fraction changes (figure 6(e)) show complex patterns that reflect both thermodynamic and dynamic responses to aerosol reductions. While convective regions show increased cloudiness (2%–5%) associated with enhanced vertical motion, some subtropical regions show decreased cloud cover due to the weakening of marine stratocumulus decks as aerosol-cloud interactions diminish. The 850 hPa circulation changes (figure 6(i)) reveal strengthened monsoon flow but also show important modifications to the subtropical anticyclones that influence moisture transport pathways. The weakening of the western Pacific subtropical high allows enhanced moisture penetration into East Asia while maintaining strong flow into South Asia, creating conditions favourable for enhanced precipitation across the broader Asian monsoon system (Wang *et al* 2012).

4.4. Summer monsoon response to east Asian aerosol reductions

The East Asian aerosol reduction experiment (ssp370-EAS126aer) examines remote influences on the South Asian monsoon using the multi-model mean from eight best-performing models.

East Asian aerosol reductions generate a markedly different response pattern over South Asia compared to local emission changes, demonstrating the role of remote aerosol forcing through atmospheric teleconnections (figure 7). The reduction in East Asian aerosol emissions creates a regional warming and circulation response that propagates downstream through modifications to the regional Walker circulation and subtropical high pressure systems, modulating the large-scale monsoon circulation in ways that generally oppose the effects of local South Asian aerosol reductions. This opposing response illustrates the complex, non-local nature of aerosol-climate interactions in the Asian monsoon system.

The AOD reduction concentrated over eastern China and the surrounding regions (figure 7(a)) drives localised surface solar radiation increases of 10–15 $W\,m^{-2}$ over East Asia (figure 7(b)), with minimal direct radiative changes over South Asia. Over the analysis domain the clear-sky and all-sky

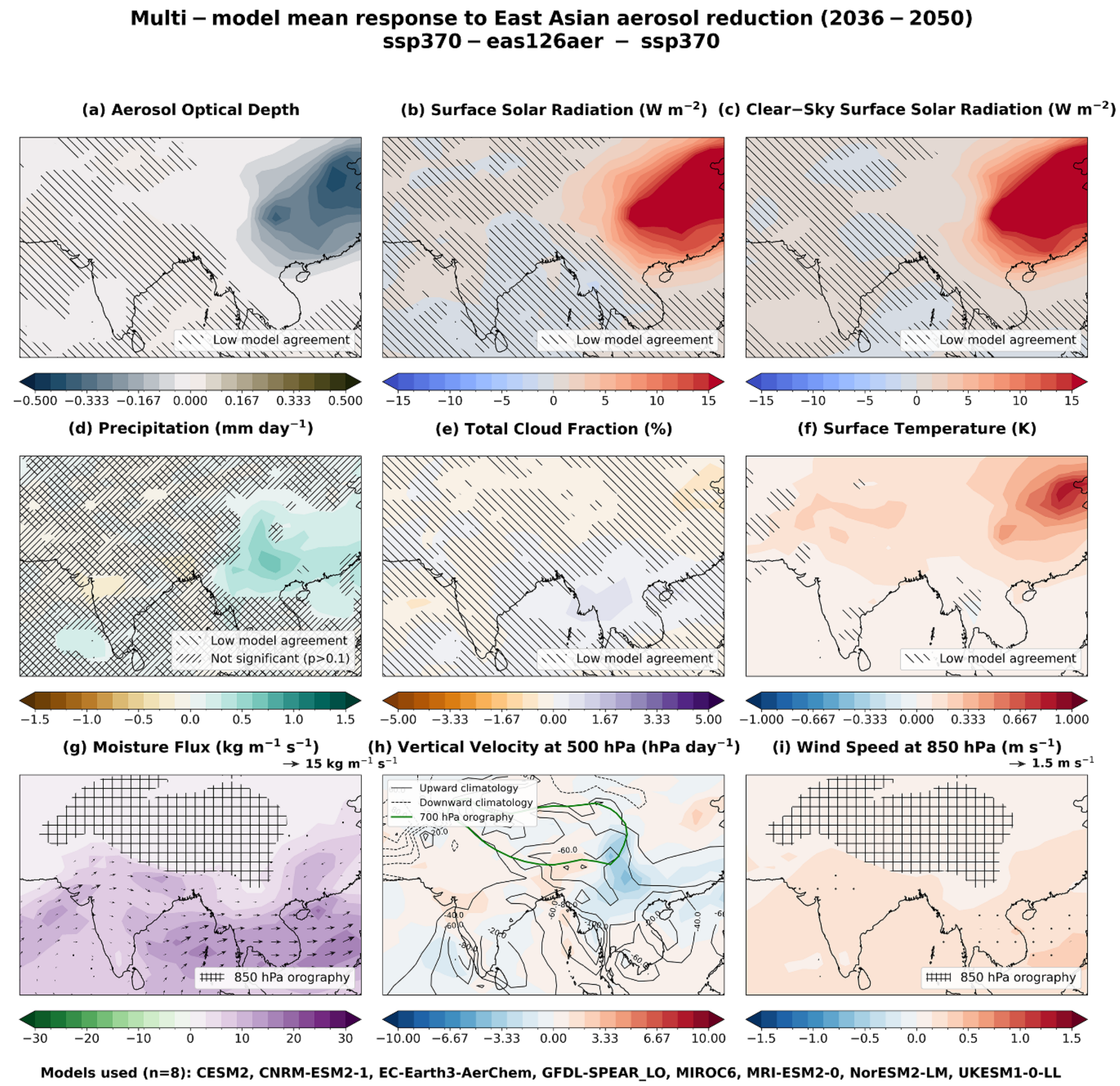

Figure 7. Multi-model mean response to East Asian aerosol reduction (ssp370-EAS126aer minus ssp370) for June-July-August 2036–2050: (a) aerosol optical depth, (b) downwelling shortwave radiation at the surface [W m^{-2}], (c) downwelling shortwave radiation at the surface (clear-sky) [W m^{-2}], (d) precipitation [mm d^{-1}], (e) total cloud fraction, (f) surface temperature [K], (g) vertically integrated horizontal moisture flux [kg m^{-1} s^{-1}], (h) vertical velocity at 500 hPa [hPa d^{-1}], (i) wind speed at 850 hPa [m s^{-1}]. Regions without hatching show where at least 70% of models agree on sign of change.

shortwave changes are again close (+2.9 versus +2.6 W m^{-2}; cloud offset ∼10%). However, the resulting surface temperature response shows warming over East Asia of 0.5–1.0 K (figure 7(f)) that triggers atmospheric circulation adjustments extending well beyond the region of aerosol change. Notably, model agreement on these East Asian responses is very strong (large areas without hatching over China), reflecting the robust near-field response to local emission reductions that all models simulate consistently. The spatial pattern of this response is similar to that found by Herbert *et al* (2021), though the multi-model consistency we observe adds confidence beyond what was shown in their single-model study.

In contrast, the South Asian precipitation response (figure 7(d)) demonstrates substantially less model consensus and exhibits a dipole pattern in some regions. Enhanced precipitation with a multi-model mean of +0.20 mm d^{-1} averaged over the East Asian domain occurs with generally positive model agreement (minimal hatching), while South Asia shows more modest reductions of 0.2–0.6 mm d^{-1} over parts of west-central and eastern regions, with extensive hatching in many places indicating poor inter-model agreement.

This asymmetry in robustness reflects fundamental differences in the physical mechanisms at play: the East Asian precipitation enhancement results directly from local surface warming and increased moisture availability (a thermodynamically-driven response that models simulate reliably), whereas the South Asian suppression depends on complex downstream circulation adjustments involving modifications to the regional Walker circulation, subtropical high position, and moisture transport pathways (dynamically-driven responses that show greater inter-model spread). Given differences in climatology across models, these teleconnections have different structure and lead to poor model agreement.

This seesaw pattern in precipitation between East and South Asia, where it occurs, has been identified in both observational analyses and modelling studies as a characteristic response to differential aerosol forcing between the regions (Zhang *et al* 2010, Salzmann *et al* 2014). The mechanism involves competition for moisture and modification of the regional Walker circulation, where enhanced convection over East Asia induces compensating subsidence over South Asia through perturbations to the regional overturning circulation. The moisture flux analysis (figure 7(g)) reveals a shift of the low-level moisture transport, with enhanced convergence over East Asia creating a moisture sink that competes with South Asian monsoon moisture demand. The strengthened East Asian monsoon circulation effectively diverts moisture that would otherwise contribute to South Asian convection, though the magnitude and spatial pattern of this diversion varies substantially across models.

The 500 hPa vertical velocity field (figure 7(h)) provides clear evidence of the seesaw mechanism in those models showing the canonical dipole response, with enhanced upward motion over East Asia accompanied by anomalous subsidence or weakened ascent over South Asia. This pattern represents a westward extension and intensification of the western Pacific subtropical high that suppresses convection over the Bay of Bengal and reduces moisture transport into the Indian subcontinent. The vertical motion dipole, where it exists, extends through the depth of the troposphere, indicating a fundamental reorganisation of the regional overturning circulation rather than shallow, localised adjustments (Li *et al* 2016).

Cloud fraction changes (figure 7(e)) mirror the precipitation and vertical motion patterns where the dipole is strongest, with increased cloudiness over East Asia (strong model agreement indicated by absence of hatching) but more ambiguous cloud responses over South Asia (extensive hatching). The overall response demonstrates that East Asian aerosol reductions, despite contributing to reduced global aerosol loading, exert complex regional influences on the South Asian monsoon through atmospheric teleconnections. These teleconnections redistribute moisture and modify the preferred regions of tropical convection (Guo *et al* 2016, Tian *et al* 2018), though the strength and even direction of these impacts show considerable model dependency.

5. Discussion and conclusions

The multi-model analysis of RAMIP experiments reveals complex and regionally heterogeneous precipitation responses to projected aerosol emission changes. South Asian aerosol reductions lead to local precipitation increases peaking at $+1.1$ mm d^{-1} over the northern Bay of Bengal and $+0.5$ mm d^{-1} over the IGP, driven by enhanced surface heating, strengthened land-sea thermal contrast, and intensified monsoon circulation. Global aerosol reductions amplify this response, with local peaks of $+1.2$ mm d^{-1} over the IGP and northern Bay of Bengal, through additional large-scale adjustments including northward ITCZ shifts and inter-hemispheric energy transport changes. East Asian aerosol reductions show robust local precipitation increases but uncertain and model-dependent effects on South Asian monsoon precipitation through atmospheric teleconnections. These findings have profound implications for the future evolution of the Indian Summer Monsoon across both pre-monsoon and peak monsoon seasons.

During the pre-monsoon period (March–May), carbonaceous aerosol reductions systematically weaken the EHP mechanism through reduced atmospheric heating over the IGP and Himalayan foothills. This EHP weakening is simulated across models with diverse physics (MIROC6 and CNRM-ESM2-1), manifesting as a coherent mid-tropospheric cooling over the foothills (up to 0.4 K) together with localised vertical-velocity anomalies that oppose the climatological upward motion; the amplitude of the response varies substantially between the two models. The pre-monsoon response is dominated by local South Asian aerosol forcing, with East Asian aerosol changes showing no systematic influence on South Asian circulation during this season. These pre-monsoon circulation adjustments set the stage for the established monsoon season (JJA), during which the magnitude, spatial pattern, and even the sign of monsoon precipitation changes depend critically on the geographic location of aerosol emission reductions, highlighting the importance of considering regional emission trajectories in addition to global mean changes when assessing future monsoon behaviour. The contrasting responses to South Asian versus East Asian aerosol reductions during the monsoon season, combined with significant inter-model diversity particularly for remote forcing, underscore both the role of atmospheric teleconnections and the remaining uncertainties in representing these interactions.

Recent modelling studies (Liu *et al* 2018, Herbert *et al* 2021) examining interactions between regional aerosol forcings provide additional context for our findings. Herbert *et al* (2021) demonstrated non-linear interactions between South and East Asian aerosol forcing under idealised large-magnitude perturbations, though the equilibrium nature and large magnitudes of their experiments require careful interpretation. Our RAMIP analysis, focusing on realistic transient emission trajectories under plausible SSP scenarios, complements these studies by examining more moderate and regionally-confined forcing changes.

Our analysis reveals substantial inter-model diversity in both baseline monsoon simulation skill and response magnitudes, consistent with the long-standing challenges in simulating the South Asian monsoon documented across CMIP generations (Sperber *et al* 2013, Choudhury *et al* 2022, Rajendran *et al* 2022). While the ensemble mean responses show physically consistent patterns aligned with theoretical understanding of aerosol-monsoon mechanisms, individual model responses span a considerable range. For the South Asian aerosol reduction experiment, precipitation increases over the IGP range from 0.3 to 1.2 mm d^{-1} across the eight best-performing RAMIP models, reflecting both differences in baseline aerosol radiative forcing (ranging from −0.75 to −1.34 W m^{-2}) and varying sensitivity of monsoon circulation to thermal forcing. Models with a stronger baseline dry bias over India generally show weaker (CanESM5-1) or altogether opposite (GISS-E2-1-G) precipitation responses to aerosol reductions, suggesting that pre-existing model biases in monsoon circulation strength may limit the simulated response to forcing changes, highlighting that continued model development to reduce systematic biases is important for improving future projections of the monsoon in response to changing emissions. The eight best-performing models identified through our evaluation demonstrate more consistent responses with enhanced magnitude, providing higher confidence in the projected monsoon enhancement under South Asian and global aerosol reductions.

The enhanced precipitation response to South Asian aerosol reductions aligns with the emerging understanding of aerosol–monsoon interactions operating through multiple pathways. As demonstrated in section 4.2, the response follows a clear causal chain. The aerosol reduction increases the clear-sky shortwave reaching the surface, warming the land and lower troposphere and raising its near-surface moist static energy (Srinivasan 2001, Boos and Kuang 2010). This strengthens the meridional tropospheric temperature gradient between the heated subcontinent and Tibetan Plateau and the cooler equatorial ocean, the dynamically relevant driver of monsoon strength (Goswami and Chakravorty 2017) rather than the local surface temperature, whose climatological correlation with Indian rainfall is in fact negative (Kothawale and Kumar 2002, Gadgil 2018). The strengthened gradient intensifies the cross-equatorial low-level (Somali) jet (Findlater 1969) and the vertically integrated moisture convergence, enhancing low-level inflow and mid-tropospheric ascent. This mechanism is further amplified by the reduction in atmospheric stability as aerosol-induced cooling aloft diminishes, allowing deeper convective development (Turner and Annamalai 2012). The EHP weakening documented in section 4.1 represents a transient pre-monsoon adjustment that ultimately gives way to enhanced monsoon circulation during peak summer months. This temporal evolution reconciles apparent contradictions between studies focusing on different seasons and highlights the importance of considering the full annual cycle when evaluating aerosol impacts (Vinoj *et al* 2014, Lau *et al* 2017).

The contrasting response to East Asian aerosol reductions reveals important complexities and uncertainties in remote aerosol forcing mechanisms. While East Asian precipitation enhancement shows robust model agreement (minimal hatching in figure 7(d), the South Asian response exhibits substantial inter-model spread (extensive hatching), with only moderate consensus on the dipole pattern. This uncertainty stems from the dynamically-mediated nature of the teleconnection, which depends on accurate simulation of the regional Walker circulation, subtropical high position, and moisture transport pathways—processes that show persistent biases and inter-model spread in current climate models. The atmospheric seesaw between East and South Asian precipitation, where robustly simulated, operates through modification of the regional Walker circulation and competitive moisture convergence, mechanisms observed in monsoon responses to ENSO phases (Kumar *et al* 2006, Wu *et al* 2008). However, the magnitude and even the presence of this seesaw shows strong model dependency, highlighting this as a key area of uncertainty requiring further investigation. This finding has critical implications for climate projections, as ongoing reductions in East Asian aerosol emissions may partially offset expected monsoon enhancement from local emission controls in South Asia, though the magnitude of this offset remains highly uncertain (Li *et al* 2017, Zhao *et al* 2019).

Upper-level dynamics further support the interpretation of a strengthened monsoon under South Asian aerosol reductions. Reduced South Asian aerosols drive enhanced deep convection over India, which releases latent heat that warms the upper troposphere, intensifying and shifting the south Asian high (SAH) northwestward (Yanai *et al* 1992, Wei *et al* (2015). An intensified SAH necessarily implies a stronger Tropical Easterly Jet along its southern flank (∼15–20°N) (Rao and Srinivasan 2016), consistent with the 200 hPa wind vector anomalies showing a coherent band of anomalous eastward flow across the Arabian Sea and Bay of Bengal in June–July. The positive meridional upper-tropospheric temperature gradient (warm over Tibet, near-neutral to the south) further drives enhanced westerly vertical wind shear through the thermal wind relationship, strengthening the surface-to-200 hPa wind reversal that characterises the active monsoon. Under East Asian aerosol reductions, the upper-level warm anomaly and anticyclonic wind curl are displaced eastward over East Asia, with no organised anticyclonic anomaly over the SAH core region, confirming that the SAH intensification is driven by local South Asian aerosol forcing rather than a remote teleconnection.

The implications of findings here extend beyond mean precipitation changes to encompass fundamental shifts in monsoon dynamics and variability. The enhanced moisture transport and strengthened circulation associated with aerosol reductions create conditions conducive to more intense rain events, even as the seasonal mean shows moderate increases (Singh *et al* 2014, Krishnan *et al* 2016). The northward shift of the monsoon precipitation zone may alter the geographic distribution of water resources, with potential enhancement over currently water-stressed regions of northwestern India but possible reductions in traditional rice-growing areas if East Asian aerosol impacts dominate (Liu *et al* 2018, Ashfaq *et al* 2021). The competing influences of regional emission changes also suggest increased uncertainty in near-term monsoon projections. The relative pace of aerosol reductions across Asia remains highly uncertain and dependent on national air quality policies, economic development pathways, and energy system transitions (Lund *et al* 2019, Samset *et al* 2019, Wilcox *et al* 2023). We further note that the present analysis addresses seasonal-mean responses; whether the enhanced mean precipitation is accompanied by changes in the number of rainy days or in heavy-precipitation frequency cannot be determined from monthly means, and quantifying these sub-seasonal statistics using the RAMIP daily output is a priority for future work.

The socioeconomic implications of these projected changes demand careful consideration in adaptation planning, recognising both the imperative for air quality improvement and the associated climate consequences. Aerosol emission reductions are essential for protecting human health, with air pollution causing millions of premature deaths annually across Asia (De Bont *et al* 2024). The direct health benefits of emission reduction programmes are substantial and largely confined to regions implementing controls. However, the climate impacts of these programmes extend well beyond national borders across regions. This creates a regional rather than national public goods issue, suggesting an important role for coordinated international approaches to emission reductions that consider both air quality and climate objectives (Herbert *et al* 2021, Persad *et al* 2022).

Enhanced monsoon precipitation under South Asian and global aerosol reduction scenarios would provide important benefits for agricultural productivity and water security, helping to reverse decades of aerosol-induced drying that has stressed water resources across the region (Burney and Ramanathan 2014, Shastri *et al* 2015). However, these benefits must be contextualised carefully: historical aerosol-induced monsoon weakening has been partially masked by greenhouse gas-driven intensification, and future scenarios involve both forcings changing simultaneously. The combined effect could drive monsoon precipitation and variability to levels exceeding the range of recent centuries, potentially overwhelming existing water management infrastructure designed for historical climate conditions.

In conclusion, this study provides a comprehensive assessment of how regional aerosol emission changes will shape the future evolution of the Indian Summer Monsoon. The RAMIP multi-model framework reveals that South Asian aerosol reductions drive robust local monsoon enhancement (multi-model mean all-India $+0.19$ mm d^{-1}) through surface warming and circulation intensification, effects that are amplified under global emission reduction scenarios (all-India $+0.28$ mm d^{-1}) through inter-hemispheric adjustments and ITCZ northward expansion. However, East Asian aerosol reductions exert an opposing but highly uncertain influence through atmospheric teleconnections. Quantitatively, global aerosol reductions strengthen the South Asian monsoon precipitation by approximately 47%–52% more than local South Asian emission reductions alone on an all-India basis. East Asian reductions show modest precipitation reductions of 0.2–0.6 mm d^{-1} over parts of west-central and eastern regions. The all-India area-mean response ranges from -0.12 to $+0.13$ mm d^{-1} across the eight models, highlighting substantial uncertainty in these remote influences.

These findings underscore the critical importance of considering spatially resolved emission trajectories and cross-regional atmospheric interactions when assessing future monsoon changes. As Asian countries pursue aggressive air quality improvements over the coming decades, understanding these complex regional interdependencies becomes essential for anticipating and adapting to the resulting hydroclimate changes. Future research priorities should include constraining aerosol-cloud interactions in monsoon environments, quantifying the role of ocean coupling in modulating atmospheric responses, and developing regionalised metrics for evaluating model performance in simulating aerosol-monsoon interactions. Only through such integrated assessments can we provide the robust projections needed to guide air quality, water resource management and climate adaptation strategies in this densely populated and climate-sensitive region.

Acknowledgment

AB acknowledges PhD studentship funding from the SCENARIO NERC Doctoral Training Partnership grant NE/S007261/1. This work used Monsoon2, a collaborative High-Performance Computing facility funded by the Met Office and the Natural Environment Research Council. This work used JASMIN, the UK collaborative data analysis facility. We acknowledge support by the Center for Advanced Study in Oslo, Norway which funded and hosted the HETCLIF centre during the academic year of 2023/24. We acknowledge the efforts of RAMIP modelling centres and data providers, the Centre for Environmental Data Analysis for archiving the data and providing access, and the multiple funding agencies who support RAMIP and CEDA. The NorESM simulations were enabled by resources provided by the National Academic Infrastructure for Supercomputing in Sweden (NAISS). We also acknowledge the following funding sources: Research Council of Norway grant 324182 (CATHY; BHS, LJW, RJA). Horizon Europe grant 101137639 (CleanCloud; BHS, LJW). The Met Office Hadley Centre Climate Programme funded by the UK government Department for Science, Innovation and Technology (FMO'C) and the European Union Horizon 2020 Research Programme ESM2025 (grant agreement number 101003536) project (FMO'C). National Science Foundation grant #AGS-2153486 (RJA). Natural Environment Research Council (NERC) grant TerraFIRMA NE/W004895/1 (LJW, PTG, STR). National Centre for Atmospheric Science, UK (LJW, STR, BNL). Environment Research and Technology Development Fund (JPMEERF20232001) of the Environmental Restoration and Conservation Agency provided by Ministry of the Environment of Japan (TK, NO). Arctic Challenge for Sustainability 3 (ArCS-3), Program Grant Number JPMXD1720251001 (TK, NO). Global Environmental Research Coordination System from Ministry of the Environment of Japan grant MLIT2253 (TK, NO). H2020 Societal Challenges grant no. 101003826 (JM, RM, DOD). Research Council Finland grant no. 337552. (JM, RM, DOD). Columbia Center for Climate and Life (DMW). Natural Sciences and Engineering Research Council of Canada (NSERC) (PK, LJF). Swedish Research Council through grant agreement no. 2022-06725 (AL). The U.S. National Oceanic and Atmospheric Administration under award NA23OAR4310601 (GP). The University of Reading Advancing the Frontiers of Earth System Prediction (AFESP) Programme under award A3720200 (SA). Climate modeling at GISS is supported by the NASA Modeling, Analysis and Prediction program, and resources supporting this work were provided by the NASA High-End Computing (HEC) Program through the NASA Center for Climate Simulation (NCCS) at Goddard Space Flight Center (KT, LN).

Data availability statement

The data that support the findings of this study will be openly available after acceptance (but before publication) at the following URL/DOI: https://doi.org/10.5285/44100d99d120487284d7b778dbc76bdf; https://catalogue.ceda.ac.uk/uuid/b7c87e4dafcc486ba1eca2abac752abf/; https://dx.doi.org/10.5285/d581329422fb455ab9af0ea96c04d266; https://dx.doi.org/10.5285/e8678aaf39144d8cb10cd02e8a562101; https://dx.doi.org/10.5285/5477E60B209A4E169CA60D7F01A017EB; https://dx.doi.org/10.5285/a33a7cc2d0a84e27a78b24d70fe257e4; https://catalogue.ceda.ac.uk/uuid/ffc25e6de67b4e3caa4693a093fd7bab/; https://catalogue.ceda.ac.uk/uuid/63233813672245a2ba3c6de90c4cfaee/; https://catalogue.ceda.ac.uk/uuid/7fbe5be720a34d4785cc7e3bb9df4641/.

Supplementary Figures available at https://doi.org/10.1088/2752-5295/ae7fad/data1.

Author contributions

Ankit Bhandekar 0009-0003-9001-5985
Conceptualization (lead), Formal analysis (lead), Investigation (lead), Methodology (lead), Visualization (lead), Writing – original draft (lead), Writing – review & editing (lead)

Laura J Wilcox 0000-0001-5691-1493
Conceptualization (supporting), Funding acquisition (lead), Investigation (supporting), Methodology (equal), Project administration (lead), Supervision (equal), Writing – original draft (supporting), Writing – review & editing (supporting)

Bryan N Lawrence 0000-0001-9262-7860
Conceptualization (supporting), Methodology (equal), Supervision (equal), Writing – original draft (supporting), Writing – review & editing (supporting)

Nathan Luke Abraham 0000-0003-3750-3544
Conceptualization (supporting), Methodology (supporting), Supervision (supporting), Writing – original draft (supporting), Writing – review & editing (supporting)

Fiona M O'Connor 0000-0003-2893-4828
Conceptualization (supporting), Methodology (supporting), Supervision (supporting), Writing – original draft (supporting), Writing – review & editing (supporting)

Bjørn H Samset 0000-0001-8013-1833
Conceptualization (supporting), Writing – review & editing (supporting)

Robert J Allen 0000-0003-1616-9719
Investigation (supporting), Writing – review & editing (supporting)

Sharar Ahmadi 0000-0002-2754-4820
Data curation (supporting), Writing – review & editing (supporting)

Annica M L Ekman 0000-0002-5940-2114
Writing – review & editing (supporting)

Maxwell T Elling 0000-0001-6091-809X
Data curation (supporting), Writing – review & editing (supporting)

Luke Fraser-Leach 0009-0003-9452-5528
Investigation (supporting), Writing – review & editing (supporting)

Paul Griffiths 0000-0002-1089-340X
Investigation (supporting), Writing – review & editing (supporting)

James Keeble 0000-0003-2714-1084
Investigation (supporting), Writing – review & editing (supporting)

Tsuyoshi Koshiro 0000-0003-2971-7446
Investigation (supporting), Writing – review & editing (supporting)

Paul Kushner 0000-0002-6404-4518
Investigation (supporting), Writing – review & editing (supporting)

Anna Lewinschal 0009-0000-9526-4524
Investigation (supporting), Writing – review & editing (supporting)

Molly MacRae 0009-0001-5734-6534
Data curation (lead), Writing – review & editing (supporting)

Risto Makkonen 0000-0002-8961-3393
Investigation (supporting), Writing – review & editing (supporting)

Joonas Merikanto 0000-0002-1145-2569
Investigation (supporting), Writing – review & editing (supporting)

Pierre Nabat 0000-0001-7034-638X
Investigation (supporting), Writing – review & editing (supporting)

Larissa Nazarenko 0000-0003-3172-9358
Writing – review & editing (supporting)

Declan O'Donnell 0000-0002-2700-471X
Investigation (supporting), Writing – review & editing (supporting)

Naga Oshima 0000-0002-8451-2411
Investigation (supporting), Writing – review & editing (supporting)

Geeta Persad 0000-0003-4690-0867
Writing – review & editing (supporting)

Steven T Rumbold 0000-0001-8138-4541
Investigation (supporting), Writing – review & editing (supporting)

Neil Swart 0000-0002-8200-6187
Investigation (supporting), Writing – review & editing (supporting)

Toshihiko Takemura 0000-0002-2859-6067
Investigation (supporting), Writing – review & editing (supporting)

Kostas Tsigaridis 0000-0001-5328-819X
Investigation (supporting), Writing – review & editing (supporting)

Daniel M Westervelt 0000-0003-0806-9961
Investigation (supporting), Writing – review & editing (supporting)

References

Adler R F *et al* 2003 The Version-2 Global Precipitation Climatology Project (GPCP) Monthly Precipitation Analysis (1979) (available at: https://journals.ametsoc.org/view/journals/hydr/4/6/1525-7541_2003_004_1147_tvgpcp_2_0_co_2.xml) (Section: 1118 Journal of Hydrometeorology)
Allen R J 2025 CESM2 output prepared for the Regional Aerosol Model Intercomparison Project (RAMIP) (https://doi.org/10.5285/fa4fe5160ca84acf919d4279fcf102c7)
Ashfaq M *et al* 2021 Robust late twenty-first century shift in the regional monsoons in RegCM-CORDEX simulations *Clim. Dyn.* **57** 1463–88
Asutosh A and Vinoj V 2024 Role of local absorbing aerosols in modulating Indian summer monsoon rainfall *Sci. Total Environ.* **910** 168663
Asutosh A, Vinoj V, Wang H, Landu K and Yoon J-H 2022 Response of Indian summer monsoon rainfall to remote carbonaceous aerosols at short time scales: teleconnections and feedbacks *Environ. Res.* **214** 113898
Barman N and Gokhale S 2023 Transported aerosols regulate the pre-monsoon rainfall over north-east India: a WRF-Chem modelling study *Atmos. Chem. Phys.* **23** 6197–215
Bauer S E, Tsigaridis K, Faluvegi G, Kelley M, Lo K K, Miller R L, Nazarenko L, Schmidt G A and Historical J W 2020 Aerosol evolution and role on climate forcing using the GISS ModelE2.1 contribution to CMIP6 *J. Adv. Model. Earth Syst.* **12** e2019MS001978
Bollasina M A, Ming Y and Ramaswamy V 2011 Anthropogenic aerosols and the weakening of the south Asian summer monsoon *Science* **334** 502–5
Boos W R and Kuang Z 2010 Dominant control of the south Asian monsoon by orographic insulation versus plateau heating *Nature* **463** 218–22
Broccoli A J, Dahl K A and Stouffer R J 2006 Response of the ITCZ to northern hemisphere cooling *Geophys. Res. Lett.* **33**
Burney J and Ramanathan V 2014 Recent climate and air pollution impacts on Indian agriculture *Proc. Natl Acad. Sci.* **111** 16319–24
Choudhury B A, Rajesh P V, Zahan Y and Goswami B N 2022 Evolution of the Indian summer monsoon rainfall simulations from CMIP3 to CMIP6 models *Clim. Dyn.* **58** 2637–62
Chung C E, Ramanathan V and Kiehl J T 2002 Effects of the south Asian absorbing haze on the northeast monsoon and surface–air heat exchange (available at: https://journals.ametsoc.org/view/journals/clim/15/17/1520-0442_2002_015_2462_eotsaa_2.0.co_2.xml) Section: Journal of Climate.
Chung E-S and Soden B J 2017 Hemispheric climate shifts driven by anthropogenic aerosol–cloud interactions *Nat. Geosci.* **10** 566–71
D'Errico M, Cagnazzo C, Fogli P G, Lau W K M, Hardenberg J von, Fierli F and Cherchi A 2015 Indian monsoon and the elevated-heat-pump mechanism in a coupled aerosol-climate model *J. Geophys. Res.: Atmos.* **120** 8712–23
Danabasoglu G 2019 NCAR CESM2 model output prepared for CMIP6 CMIP historical (https://doi.org/10.22033/ESGF/CMIP6.7627)
Danabasoglu G *et al* 2020 The Community Earth System Model Version 2 (CESM2) *J. Adv. Model. Earth Syst.* **12** e2019MS001916
Dave P, Bhushan M and Venkataraman C 2017 Aerosols cause intraseasonal short-term suppression of Indian monsoon rainfall *Sci. Rep.* **7** 17347
De Bont J *et al* 2024 Ambient air pollution and daily mortality in ten cities of India: a causal modelling study *Lancet Planet. Health* **8** e433–40
Delworth T L *et al* 2020 SPEAR: the next generation gfdl modeling system for seasonal to multidecadal prediction and projection *J. Adv. Model. Earth Syst.* **12** e2019MS001895
Dey S and Di Girolamo L 2011 A decade of change in aerosol properties over the Indian subcontinent *Geophys. Res. Lett.* **38**
EC-Earth-Consortium 2019 EC-Earth-Consortium EC-Earth3 model output prepared for CMIP6 CMIP historical (https://doi.org/10.22033/ESGF/CMIP6.4700)
Eyring V *et al* 2016 Overview of the Coupled Model Intercomparison Project Phase 6 (CMIP6) experimental design and organization *Geosci. Model Dev.* **9** 1937–58
Fadnavis S, Chavan P, Thaware R and Tilmes S 2024 Amplified drying in south Asian summer monsoon precipitation due to anthropogenic sulfate aerosols *Environ. Pollut.* **343** 123175
Fan J, Wang Y, Rosenfeld D and Liu X 2016 Review of aerosol–cloud interactions: mechanisms, significance and challenges *J. Atmos. Sci.* **73** 4221–52

Findlater J 1969 A major low-level air current near the Indian Ocean during the northern summer *Q. J. R. Meteorol. Soc.* **95** 362–80
Fraser-Leach L, Kushner P, von Salzen K and Swart N 2025 CanESM5-1 output prepared for the Regional Aerosol Model Intercomparison Project (RAMIP) (https://doi.org/10.5285/a33a7cc2d0a84e27a78b24d70fe257e4)
Gadgil S 2018 The monsoon system: land–sea breeze or the ITCZ? *J. Earth Syst. Sci.* **127** 1
Goswami B N and Chakravorty S 2017 Dynamics of the Indian Summer Monsoon Climate *Oxford Research Encyclopedia of Climate Science*, ed H von Storch (Oxford University Press)
Guo L, Turner A G and Highwood E J 2016 Local and remote impacts of aerosol species on indian summermonsoon rainfall in a GCM (available at: https://journals.ametsoc.org/view/journals/clim/29/19/jcli-d-15-0728.1.xml)
He L, Zhou T and Chen X 2023 South Asian summer rainfall from CMIP3 to CMIP6 models: biases and improvements *Clim. Dyn.* **61** 1049–61
Herbert R, Wilcox L J, Joshi M, Highwood E and Frame D 2021 Nonlinear response of Asian summer monsoon precipitation to emission reductions in South and East Asia *Environ. Res. Lett.* **17** 014005
Hwang Y–T, Frierson D M W and Kang S M 2013 Anthropogenic sulfate aerosol and the southward shift of tropical precipitation in the late 20th century *Geophys. Res. Lett.* **40** 2845–50
Jin Q and Wang C 2017 A revival of Indian summer monsoon rainfall since 2002 *Nat. Clim. Change* **7** 587–94
Jin Q, Wei J and Yang Z-L 2014 Positive response of indian summer rainfall to middle east dust *Geophys. Res. Lett.* **41** 4068–74
Jin Q, Yang Z-L and Wei J 2016 High sensitivity of indian summer monsoon to middle east dust absorptive properties *Sci. Rep.* **6** 30690
Kelley M *et al* 2020 GISS-E21: configurations and climatology *J. Adv. Model. Earth Syst.* **12** e2019MS002025
Kothawale D R and Kumar K R 2002 Tropospheric temperature variation over India and links with the Indian summer monsoon : 1971-2000 *Mausam* **53** 289–308
Krishnan R, Sabin T P, Vellore R, Mujumdar M, Sanjay J, Goswami B N, Hourdin F, Dufresne J-L and Terray P 2016 Deciphering the desiccation trend of the south Asian monsoon hydroclimate in a warming world *Clim. Dyn.* **47** 1007–27
Kumar K K, Rajagopalan B, Hoerling M, Bates G and Cane M 2006 Unraveling the mystery of indian monsoon failure during El Niño *Science* **314** 115–9
Lau K M and Kim K M 2006 Observational relationships between aerosol and Asian monsoon rainfall and circulation *Geophys. Res. Lett.* **33** 2006GL027546
Lau K M, Kim M K and Kim K M 2006 Asian summer monsoon anomalies induced by aerosol direct forcing: the role of the Tibetan Plateau *Clim. Dyn.* **26** 855–64
Lau W K M, Kim K-M, Shi J-J, Chin M, Tan Q, Peters-Lidard C and Tao W K 2017 Impacts of aerosol–monsoon interaction on rainfall and circulation over northern india and the Himalaya foothills *Clim. Dyn.* **49** 1945–60
Lewinschal A 2025 NorESM2-LM output prepared for the Regional Aerosol Model Intercomparison Project (RAMIP) (https://doi.org/10.5285/44100d99d120487284d7b778dbc76bdf)
Li Z *et al* 2016 Aerosol and monsoon climate interactions over Asia *Rev. Geophys.* **54** 866–929
Li Z, Rosenfeld D and Fan J 2017 Aerosols and Their Impact on Radiation, Clouds, Precipitation and Severe Weather Events *Oxford Research Encyclopedia of Environmental Science.*
Liu L *et al* 2018 A PDRMIP multimodel study on the impacts of regional aerosol forcings on global and regional precipitation *J. Clim.* **31** 4429–47
Liu Z, Bollasina M A and Wilcox L J 2024 Impact of Asian aerosols on the summer monsoon strongly modulated by regional precipitation biases *Atmos. Chem. Phys.* **24** 7227–52
Lund M T, Myhre G and Samset B H 2019 Anthropogenic aerosol forcing under the shared socioeconomic pathways *Atmos. Chem. Phys.* **19** 13827–39
Miller R L *et al* 2021 CMIP6 historical simulations (1850–2014) With GISS-E21 *J. Adv. Model. Earth Syst.* **13** e2019MS002034
Nabat P 2025 CNRM-ESM2-1 output prepared for the Regional Aerosol Model Intercomparison Project (RAMIP) (https://doi.org/10.5285/5477E60B209A4E169CA60D7F01A017EB)
NASA/GISS 2018 NASA-GISS GISS-E21G model output prepared for CMIP6 CMIP historical (available at: https://doi.org/10.22033/ESGF/CMIP6.7127)
NOAA Geophysical Fluid Dynamics Laboratory 2020 SPEAR (Seamless system for prediction and EArth system research) model output (available at: www.gfdl.noaa.gov/spear_large_ensembles/) Published: Downloaded from GFDL NOMADS server
O'Donnell D, Makkonen R and Merikanto J 2025 EC-Earth3-AerChem output prepared for the Regional Aerosol Model Intercomparison Project (RAMIP) (https://doi.org/10.5285/d581329422fb455ab9af0ea96c04d266)
Oshima N and Koshiro T 2025 MRI-ESM2-0 output prepared for the Regional Aerosol Model Intercomparison Project (RAMIP) (https://doi.org/10.5285/e8678aaf39144d8cb10cd02e8a562101)
Pai D S, Rajeevan M, Sreejith O P, Mukhopadhyay B and Satbha N S 2014 Development of a new high spatial resolution ($0.25° \times 0.25°$) long period (1901-2010) daily gridded rainfall data set over India and its comparison with existing data sets over the region *Mausam* **65** 1–18
Paynter D J 2025 GFDL-SPEAR_lo output prepared for the Regional Aerosol Model Intercomparison Project (RAMIP) (available at: http://catalogue.ceda.ac.uk/uuid/bd3bdca3c9a24553893cafffe768fe56/)
Persad G G 2023 The dependence of aerosols' global and local precipitation impacts on the emitting region *Atmos. Chem. Phys.* **23** 3435–52
Persad G G, Samset B H and Wilcox L J 2022 Aerosols must be included in climate risk assessments *Nature* **611** 662–4
Quaas J *et al* 2022 Robust evidence for reversal of the trend in aerosol effective climate forcing *Atmos. Chem. Phys.* **22** 12221–39
Rajeevan M and Srinivasan J 2000 Net Cloud radiative forcing at the top of the atmosphere in the Asian monsoon region *J. Clim.* **13** 650–7
Rajendran K, Surendran S, Varghese S J and Sathyanath A 2022 Simulation of Indian summer monsoon rainfall, interannual variability and teleconnections: evaluation of CMIP6 models *Clim. Dyn.* **58** 2693–723
Ramanathan V, Chung C, Kim D, Bettge T, Buja L, Kiehl J T, Washington W M, Fu Q, Sikka D R and Wild M 2005 Atmospheric brown clouds: impacts on south Asian climate and hydrological cycle *Proc. Natl Acad. Sci.* **102** 5326–33
Rao S and Srinivasan J 2016 The impact of latent heating on the location and strength of the tropical easterly jet *Meteorol. Atmos. Phys.* **128** 247–61
Riahi K *et al* 2017 The Shared Socioeconomic Pathways and their energy, land use and greenhouse gas emissions implications: an overview *Glob. Environ. Change* **42** 153–68

Rumbold S T, Ahmadi S, Wilcox L J, Keeble J, Griffiths P T, Predoi V, Lister G and Hatcher R 2025 UKESM1-0-LL output prepared for the Regional Aerosol Model Intercomparison Project (RAMIP) (available at: https://catalogue.ceda.ac.uk/uuid/63233813672245a2ba3c6de90c4cfaee/)

Salzmann M, Weser H and Cherian R 2014 Robust response of Asian summer monsoon to anthropogenic aerosols in CMIP5 models *J. Geophys. Res.: Atmos.* **119** 11321–37

Samset B H, Lund M T, Bollasina M, Myhre G and Wilcox L 2019 Emerging Asian aerosol patterns *Nat. Geosci.* **12** 582–4

Sarangi C, Tripathi S N, Mishra A K, Goel A and Welton E J 2016 Elevated aerosol layers and their radiative impact over Kanpur during monsoon onset period *J. Geophys. Res.: Atmos.* **121** 7936–57

Schneider U, Becker A, Finger P, Meyer-Christoffer A, Ziese M and Rudolf B 2014 GPCC's new land surface precipitation climatology based on quality-controlled in situ data and its role in quantifying the global water cycle *Theor. Appl. Climatol.* **115** 15–40

Seferian R 2018 CNRM-CERFACS CNRM-ESM2-1 model output prepared for CMIP6 CMIP historical (https://doi.org/10.22033/ESGF/CMIP6.4068)

Séférian R *et al* 2019 Evaluation of CNRM earth system model, CNRM-ESM2-1: role of earth system processes in present-day and future climate *J. Adv. Model. Earth Syst.* **11** 4182–227

Seland øyvind *et al* 2020 Overview of the Norwegian Earth System Model (NorESM2) and key climate response of CMIP6 DECK, historical and scenario simulations *Geosci. Model Dev.* **13** 6165–200

Seland yvind *et al* 2019 NCC NorESM2-LM model output prepared for CMIP6 CMIP historical (https://doi.org/10.22033/ESGF/CMIP6.8036)

Sellar A A *et al* 2019 UKESM1: Description and Evaluation of the U.K. Earth System Model *J. Adv. Model. Earth Syst.* **11** 4513–58

Shastri H, Paul S, Ghosh S and Karmakar S 2015 Impacts of urbanization on Indian summer monsoon rainfall extremes *J. Geophys. Res.: Atmos.* **120** 496–516

Shawki D, Voulgarakis A, Chakraborty A, Kasoar M and Srinivasan J 2018 The South Asian Monsoon Response to Remote Aerosols: Global and Regional Mechanisms *J. Geophys. Res.: Atmos.* **123** 11585–01

Singh D, Tsiang M, Rajaratnam B and Diffenbaugh N S 2014 Observed changes in extreme wet and dry spells during the South Asian summer monsoon season *Nat. Clim. Change* **4** 456–61

Sperber K R, Annamalai H, Kang I-S, Kitoh A, Moise A, Turner A, Wang B and Zhou T 2013 The Asian summer monsoon: an intercomparison of CMIP5 vs. CMIP3 simulations of the late 20th century *Clim. Dyn.* **41** 2711–44

Srinivasan J 2001 A simple thermodynamic model for seasonal variation of monsoon rainfall *Curr. Sci.* **80** 73–77 (available at: http://www.jstor.org/stable/24105558)

Stier P *et al* 2024 Multifaceted aerosol effects on precipitation *Nat. Geosci.* **17** 719–32

Swart N C *et al* 2019a The Canadian Earth System Model version 5 (CanESM5.0.3) *Geosci. Model Dev.* **12** 4823–73

Swart N C *et al* 2019b CCCma CanESM5 model output prepared for CMIP6 CMIP historical (https://doi.org/10.22033/ESGF/CMIP6.3610)

Takemura T 2025 MIROC6 output prepared for the Regional Aerosol Model Intercomparison Project (RAMIP) (available at: https://catalogue.ceda.ac.uk/uuid/7fbe5be720a34d4785cc7e3bb9df4641/)

Tang Y, Rumbold S, Ellis R, Kelley D, Mulcahy J, Sellar A, Walton J and Jones C 2019 MOHC UKESM1.0-LL model output prepared for CMIP6 CMIP historical (available at: https://doi.org/10.22033/ESGF/CMIP6.6113)

Tatebe H *et al* 2019 Description and basic evaluation of simulated mean state, internal variability and climate sensitivity in MIROC6 *Geosci. Model Dev.* **12** 2727–65

Tatebe H and Watanabe M 2018 MIROC MIROC6 model output prepared for CMIP6 CMIP historical (available at: https://doi.org/10.22033/ESGF/CMIP6.5603)

Tian F, Dong B, Robson J and Sutton R 2018 Forced decadal changes in the east Asian summer monsoon: the roles of greenhouse gases and anthropogenic aerosols *Clim. Dyn.* **51** 3699–715

Trenberth K E and Shea D J 2005 Relationships between precipitation and surface temperature *Geophys. Res. Lett.* **32**

Turner A G and Annamalai H 2012 Climate change and the South Asian summer monsoon *Nat. Clim. Change* **2** 587–95

van Noije T *et al* 2021 EC-Earth3-AerChem: a global climate model with interactive aerosols and atmospheric chemistry participating in CMIP6 *Geosci. Model Dev.* **14** 5637–68

Vinoj V, Rasch P J, Wang H, Yoon J-H, Ma P-L, Landu K and Singh B 2014 Short-term modulation of Indian summer monsoon rainfall by West Asian dust *Nat. Geosci.* **7** 308–13

Voigt A, Pincus R, Stevens B, Bony S, Boucher O, Bellouin N, Lewinschal A, Medeiros B, Wang Z and Zhang H 2017 Fast and slow shifts of the zonal-mean intertropical convergence zone in response to an idealized anthropogenic aerosol *J. Adv. Model. Earth Syst.* **9** 870–92

Wang B, Liu J, Kim H-J, Webster P J and Yim S-Y 2012 Recent change of the global monsoon precipitation (1979–2008) *Clim. Dyn.* **39** 1123–35

Wang C, Soden B J, Yang W and Vecchi G A 2021 Compensation between cloud feedback and aerosol-cloud interaction in CMIP6 models *Geophys. Res. Lett.* **48** e2020GL091024

Wang H, Xie S-P, Kosaka Y, Liu Q and Du. Y 2019 Dynamics of Asian summer monsoon response to anthropogenicaerosol forcing (available at: https://journals.ametsoc.org/view/journals/clim/32/3/jcli-d-18-0386.1.xml) Section: Journal of Climate

Wang P, Yang Y, Xue D, Ren L, Tang J, Ruby Leung L and Liao H 2023 Aerosols overtake greenhouse gases causing a warmer climate and more weather extremes toward carbon neutrality *Nat. Commun.* **14** 7257

Wei W, Zhang R, Wen M, Kim B-J and Nam J-C 2015 Interannual variation of the south Asian high and itsrelation with indian and east Asian summer monsoon rainfall *J. Clim.* **28** 2623–34

Westervelt D M, Tsigaridis K, Nazarenko L S and Elling M T 2025 GISS-E2-1-G output prepared for the Regional Aerosol Model Intercomparison Project (RAMIP) (available at: https://catalogue.ceda.ac.uk/uuid/ffc25e6de67b4e3caa4693a093fd7bab/)

Westervelt D M, You Y, Li X, Ting M, Lee D E and Ming Y 2020 Relative Importance of Greenhouse Gases, Sulfate, Organic Carbon and Black Carbon Aerosol for South Asian Monsoon Rainfall Changes *Geophys. Res. Lett.* **47** e2020GL088363

Wilcox L J *et al* 2020 Accelerated increases in global and Asian summer monsoon precipitation from future aerosol reductions *Atmos. Chem. Phys.* **20** 11955–77

Wilcox L J *et al* 2023 The Regional Aerosol Model Intercomparison Project (RAMIP) *Geosci. Model Dev.* **16** 4451–79

Wilcox L J 2025 *Opinion: The Role of Aerchemmip in Advancing Climate and Air Quality Research.* (OSF)

Wu R, Kirtman B P and Krishnamurthy V 2008 An asymmetric mode of tropical Indian Ocean rainfall variability in boreal spring *J. Geophys. Res.: Atmos.* **113** D5

Xiang B, Xie S-P, Kang S M and Kramer R J 2023 An emerging Asian aerosol dipole pattern reshapes the Asian summer monsoon and exacerbates northern hemisphere warming *npj Clim. Atmos. Sci.* **6** 77

Yanai M, Li C and Song Z 1992 Seasonal heating of the Tibetan Plateau and its effects on the evolution of the Asian summer monsoon *J. Meteorol. Soc. Japan II* **70** 319–51

Yatagai A, Kamiguchi K, Arakawa O, Hamada A, Yasutomi N and APHRODITE A K 2012 Constructing a long-term daily gridded precipitation dataset for asia based on a dense network of rain gauges (available at: https://journals.ametsoc.org/view/journals/bams/93/9/bams-d-11-00122.1.xml)

Yukimoto S *et al* 2019a The meteorological research institute earth system model version 2.0, MRI-ESM2.0: description and basic evaluation of the physical component *J. Meteorol. Soc. Japan II* **97** 931–65

Yukimoto S *et al* 2019b MRI MRI-ESM2.0 model output prepared for CMIP6 CMIP historical (available at: https://doi.org/10.22033/ESGF/CMIP6.6842)

Zhang Li, Liao H and Li. J 2010 Impacts of Asian summer monsoon on seasonal and interannual variations of aerosols over eastern China *J. Geophys. Res.: Atmos.* **115**

Zhao A, Stevenson D S and Bollasina M A 2019 Climate Forcing and Response to Greenhouse Gases, Aerosols and Ozone in CESM1 *J. Geophys. Res.: Atmos.* **124** 13876–94